Comparisons of Aerodynamic Data with the Main Wind Force–Resisting System Provisions of ASCE 7-16. I: Low-Rise Buildings

Jin Wang, S.M.ASCE[1]; and Gregory A. Kopp, M.ASCE[2]

Downloaded from ascelibrary.org by University of Western Ontario on 09/05/22. Copyright ASCE. For personal use only; all rights reserved.

Abstract: This study assesses the wind load provisions for low-rise buildings with Chapters 27 and 28 in ASCE 7-16 and analyzes the dependence of the aerodynamics on the building geometric parameters. A systematic analysis of an aerodynamic database was used for this purpose. The mean and gust-factored uplift, base shear, and area-averaged wall pressure coefficients acting on the building surfaces comprise the main focus of this work. The results indicate that Chapter 27 captures the increasing tendency of roof uplift coefficients with larger roof heights reasonably well. The base shear obtained from the database is observed to vary with roof height, but conflicts with the design wind loads of ASCE 7-16. The ratio of roof height, H, to the horizontal plan dimension parallel to wind direction, L, is the critical nondimensional geometric parameter to model the uplift, leeward wall, and side wall pressure trends for low-rise buildings. It is also observed that the uplift can be used as a predictor of the side wall pressure coefficients for low-rise buildings. The Chapter 28 provisions conservatively envelop the data for relatively low buildings, but underestimate the wind loads for $H/L > 0.5$. **DOI: 10.1061/(ASCE)ST.1943-541X.0002925.** © *2020 American Society of Civil Engineers.*

Author keywords: Wind loads; Building aerodynamics; Low-rise buildings; ASCE 7.

Introduction

ASCE 7-16 (ASCE 2016) has six chapters that each cover and describe different aspects of the wind load provisions, including alternative methods for assessing wind loads. Chapter 26 provides the basic wind design parameters, including definitions, basic wind speeds, exposure categories, internal pressures, elevation effects, enclosure classification, gust effects, and topographic factors. A 3-s gust has been adopted as the basic design wind speed in ASCE 7 since 1995. The design wind loads in ASCE 7-16 can be categorized into two groups based on the building elements of interest: (1) Main Wind Force–Resisting System (MWFRS) in three chapters, where the Directional Procedure for buildings of all heights is provided by Chapter 27, the Envelop Procedure for low-rise buildings is given in Chapter 28, and the Directional Procedure for building appurtenances and other structures is given in Chapter 29; and (2) Components and Cladding (C&C) for effective wind areas smaller than 65 m^2 in Chapter 30. Chapter 31 describes the requirements for the Wind Tunnel Procedure for all buildings and other structures. The main difference in the three chapters focusing primarily on building loads (Chapters 27, 28 and 30) is in the external pressure coefficients. All the internal pressure coefficients provided in this standard are gust-factored peak values, which depend on the enclosure classification. It is worth mentioning that the pressure coefficients do not vary with terrain in ASCE 7-16, such that terrain is assumed to only affect the gust wind speeds but not the building aerodynamics.

The major difference between Chapters 27 and 28 is the approach to determining the peak wind loads. A gust-effect factor, G, multiplied by a mean external pressure, determines the peak load coefficient in Chapter 27. The gust-effect factor was developed based on the work of Solari (1993a, b) and Solari and Kareem (1998), by translating the dynamic amplification of the loading caused by the atmospheric turbulence and dynamic sensitivity of the structure into an equivalent static load. This approach explicitly makes use of the quasi-steady theory. Thus, body-generated turbulence effects are not included. ASCE 7-95 (ASCE 1995) required the gust-effect factor, G, to be 0.8 for exposures A (urban) and B (suburban) and 0.85 for exposure C (open country) and D (open water). These values were obtained by reducing the actual gust-effect factor by a factor of 0.925 to adjust the loads to be closer to those of ASCE 7-93 (Solari and Kareem 1998). Since ASCE 7-02 (ASCE 2002), the value of $G = 0.85$ is permitted without calculation for rigid buildings in all terrains. In the case of flexible buildings and other structures, the gust-effect factor for the MWFRS is obtained by an analysis that incorporates the dynamic properties of the structure. It is noted that low-rise buildings are generally treated as being rigid.

As mentioned earlier, Chapter 27 utilizes mean pressure coefficients. For walls, these are coefficients averaged over the entire walls (noting the additional discussion below for windward walls). For low-slope roofs, the roof area is broken into either two zones or three zones (there are actually four zones, but two of these are adjacent with exactly the same coefficients), which depend on H/L, where H is the roof height and L is the length of the building. The roof zones sizes depend on H, consistent with the recent changes made to the C&C low-slope roof pressure coefficients (Kopp and Morrison 2018).

In contrast to Chapter 27, Chapter 28 uses directly obtained peak pressure coefficients, $[GCp]$. Only low-rise buildings were used in the development of this method, where a low-rise building

[1]Postdoctoral Associate, Boundary Layer Wind Tunnel Laboratory, Faculty of Engineering, Univ. of Western Ontario, London, ON, Canada N6A 5B9. Email: jwan2225@uwo.ca

[2]Professor, Boundary Layer Wind Tunnel Laboratory, Faculty of Engineering, Univ. of Western Ontario, London, ON, Canada N6A 5B9 (corresponding author). Email: gakopp@uwo.ca; gak@blwtl.uwo.ca

Note. This manuscript was submitted on May 12, 2020; approved on September 22, 2020; published online on December 21, 2020. Discussion period open until May 21, 2021; separate discussions must be submitted for individual papers. This paper is part of the ***Journal of Structural Engineering***, © ASCE, ISSN 0733-9445.

is defined as one with a mean roof height less than 18.3 m and that does not exceed the least horizontal dimension. No geometric dependence on the $[GCp]$ values is provided, except for the size of the edge zones on the roof and walls, which are assumed to depend on both the plan dimensions and building height. As with Chapter 27, these pressure coefficients are used in all terrains. However, unlike for the development of the gust-effect factor, no assumption regarding the quasi-steady theory is made in how the pressure coefficients were obtained. Thus, body-generated turbulence effects are implicitly included.

Similar to Chapter 27, Chapter 28 buildings must be designed for all wind directions. Chapter 28 provides two load cases (Case A and Case B), including eight corner wind directions, to envelop the desired structural actions (bending moment, shear, thrust). Case A is regarded as the critical normal-to-ridge wind case, while Case B is regarded as the critical parallel-to-ridge case. The load cases are equivalent static loads that envelop the expected structural actions for low-rise buildings, such as the bending moments at the knees of frames, bay loads for metal building systems, etc.

Another notable difference between Chapters 27 and 28 is the selection of velocity pressure exposure coefficient, K_Z. Both Chapters 28 and 30 adopt K_Z at roof height for external (and internal) pressures. In contrast, in Chapter 27, the local elevation is used for the windward wall, while the roof height is assumed for the leeward wall, side wall, and roof. Note that ASCE 7 defines mean roof height as the average of the eave height and the height to the highest point on the roof surface (except for roof slopes less than or equal to 10°, where the mean roof height is permitted to be taken as the eave height). To convert the local elevation velocity pressure, an adjustment factor, F_c, can be applied, as follows:

$$F_c = \frac{\int_0^H K_Z dz}{H \times K_H} \tag{1}$$

where K_Z = local velocity pressure; and K_H = velocity pressure at mean roof height. This can be obtained either based on the tabulated values in Tables 26.10-1 or Eqs. C26.10-1 and C26.10-2. Note that the K_Z values below 9.1 m for Exposure B in Chapter 28 are different from those used in other chapters. In the present

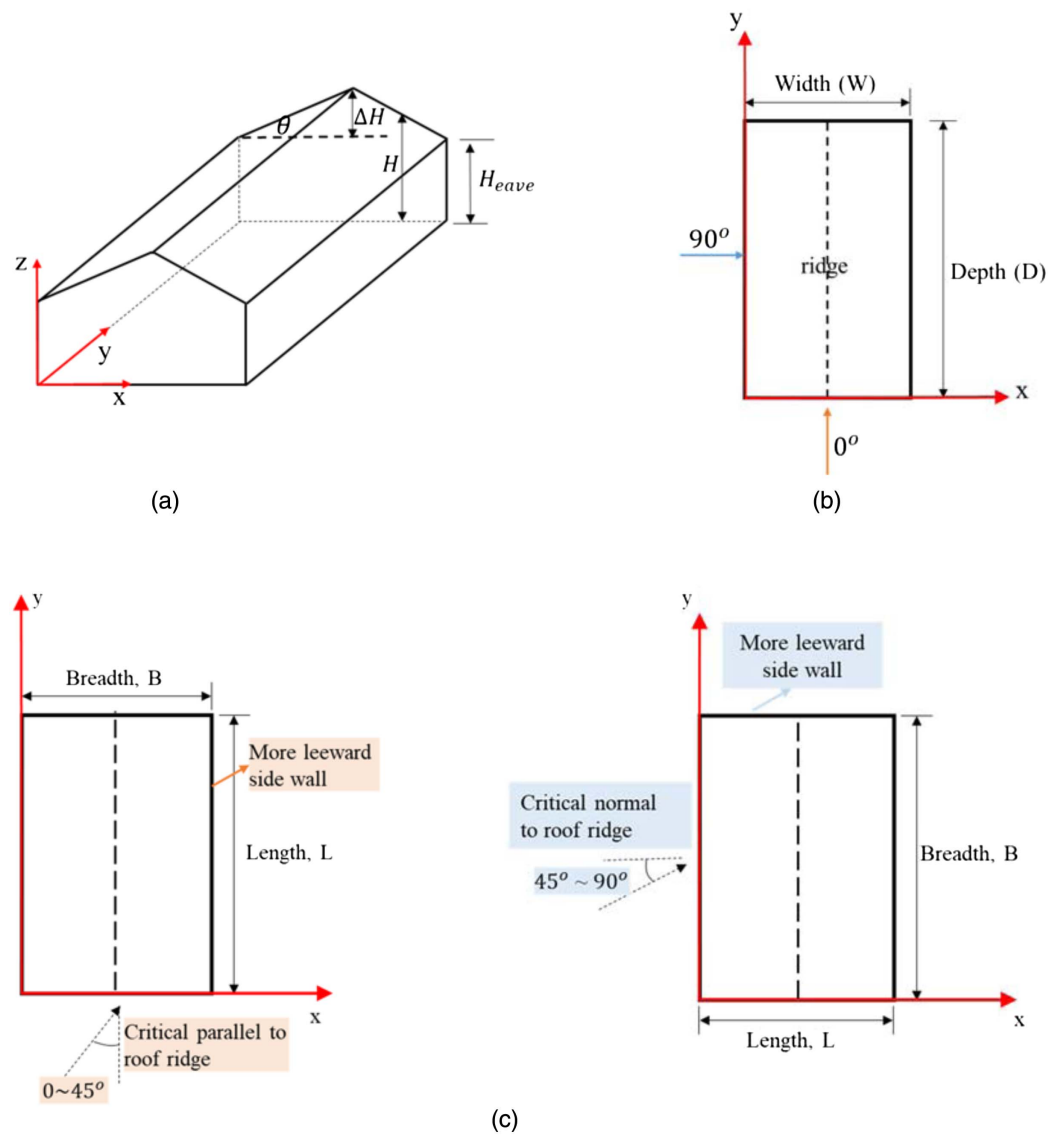

Fig. 1. Definition sketch of model dimensions: (a) 3D view of the building; (b) plan view of the building; and (c) definition of length (L) and breadth (B).

Downloaded from ascelibrary.org by University of Western Ontario on 09/05/22. Copyright ASCE. For personal use only; all rights reserved.

study, we uniformly employed the values used in Chapter 27 to make comparisons.

The aerodynamic coefficients for the overall wind loads on buildings in ASCE 7-16 are largely based primarily on experimental work carried out by Akins et al. (1977), Davenport et al. (1977), and Stathopoulos (1979). Reviews and examinations of current prevailing international standards have been provided by Kasperski (1996), Chiu and Perry (1997), Stathopoulos (2003), Holmes et al. (2009, 2014), and Simiu et al. (2012). A special issue of the *Journal of Wind and Structures* in 2005 published five papers in which all aspects of codification for wind loads were reviewed (Holmes et al. 2005a, b; Kasperski and Geurts 2005; Letchford et al. 2005; Tamura et al. 2005). These papers recommended that further investigations are needed regarding codification of wind loads. Given the differences in approach for the development of the provisions in Chapters 27 and 28, it is perhaps not surprising that they lead to quite different wind loads for low-rise buildings. However, a detailed analysis of these differences has not been conducted, even though they are based on data that are more than 40 years old.

Significant advances have been made in measurement technology and our understanding of full-scale wind loads. In particular, full-scale field studies, such as those at Texas Tech University (e.g., Levitan and Mehta 1992), have changed the methodologies of wind tunnel tests, as explained by St. Pierre et al. (2005), Tieleman (2003), and Lopez and Masters (2010). Previous studies using current methods (e.g., Ho et al. 2005) have shown that the tabulated peak pressure coefficients, corresponding to Chapter 28 of ASCE 7-16, tend to underestimate the design wind loads compared with the wind tunnel results (St. Pierre et al. 2005, who only used a subset of the database of Ho et al. 2005). Gavanski and Uematsu (2014) examined various building parameters and found that some of the current code provisions may be too low for the local (C&C) wind pressures on the walls of low-rise buildings in Chapter 30, although values for several model geometries were slightly overestimated for large effective wind areas. Kopp and Morrison (2018) examined the wind load provisions for local area-averaged pressures in ASCE 7-10 for low-rise building roofs, which led to the changes (increases for relatively small effective wind areas but decreases for large areas) in Chapter 30 of ASCE 7-16. In addition, Liu et al. (2019) experimentally studied the wind loads on high-rise buildings, and found that the measured peak pressure coefficients exceed the provisions of Chapter 27 due to the mismatch of both the mean pressure coefficients and the gust-effect factor for rigid buildings. However, a detailed assessment of both Chapters 27 and 28 has not been

Table 1. Summary of the building geometries from NIST database

Group no.	Building no.	Model no. (NIST database) Open	Suburban	Roof slope (tangent)	Roof slope, θ (degrees)	Width, W (m)	Depth, D (m)	Eave height, H_{eave} (m)	Length scale
(a)	1	EH1	EH2	1/12	4.8	24.38	38.1	12.19	1/100
	2	EG1	EG2					9.75	
	3	EF1	EF2					7.32	
	4	EE1	EE2					4.88	
(b)	5	IM1	IM2	1/48	1.2	24.38	38.1	12.19	1/100
	6	IL1	IL2					9.75	
	7	IK1	IK2					7.32	
	8	IJ1	IJ2					5.49	
	9	II1	II2					3.66	
(c)	10	JP1	JP2	1/12	4.8	12.19	19.05	12.19	1/100
	11	JO1	JO2					7.32	
	12	JN1	JN2					5.49	
	13	JM1	JM2					3.66	
(d)	14	OX1	OX2	1/12	4.8	48.77	76.2	12.19	1/100
	15	OW1	OW2					7.32	
	16	OV1	OV2					5.49	
	17	OU1	OU2					3.66	
(e)	18	P51	P52	1/12	4.8	36.58	57.15	12.19	1/100
	19	P41	P42					7.32	
	20	P31	P32					5.49	
	21	P21	P22					4.88	
	22	P11	P12					3.66	
(f)	23	Q21	Q22	1/24	2.4	30.48	60.96	9.75	1/200
	24	Q11	Q12					6.1	
(g)	25	T21	T22	1/24	2.4	15.24	30.48	4.88	1/100
	26	T11	T12					3.66	
(h)	27	V21	V22	1/24	2.4	15.24	53.34	4.88	1/100
	28	V11	V12					3.66	
(i)	29	M41	M42	3/12	14	24.38	38.1	12.19	1/100
	30	M31	M32					9.75	
	31	M21	M22					7.32	
	32	M11	M12					4.88	
(j)	33	Y41	Y42	6/12	27	24.38	38.1	12.19	1/100
	34	Y31	Y32					7.32	
	35	Y21	Y22					5.49	
	36	Y11	Y12					3.66	

Source: Data from Ho et al. (2005).

Downloaded from ascelibrary.org by University of Western Ontario on 09/05/22. Copyright ASCE. For personal use only; all rights reserved.

conducted, particularly regarding the variation of the wind loads with respect to the geometric parameters that define the building shape. The objective of the current work is to do this assessment, using a large, consistent, and modern database.

Due to length requirements, we have split this work into two parts so that the analysis, discussion, and conclusions could be clearly presented. Part I focuses on low-rise buildings, which are the subject of both Chapters 27 and 28. Part II focuses on mid- and high-rise buildings, which are only considered in Chapter 27; however, the difference in methods between the two chapters are also assessed in Part II. In addition, this study places particular emphasis on the roles of key geometric parameters that affect both mean and peak loads so that the possibility of a unified method may also be assessed.

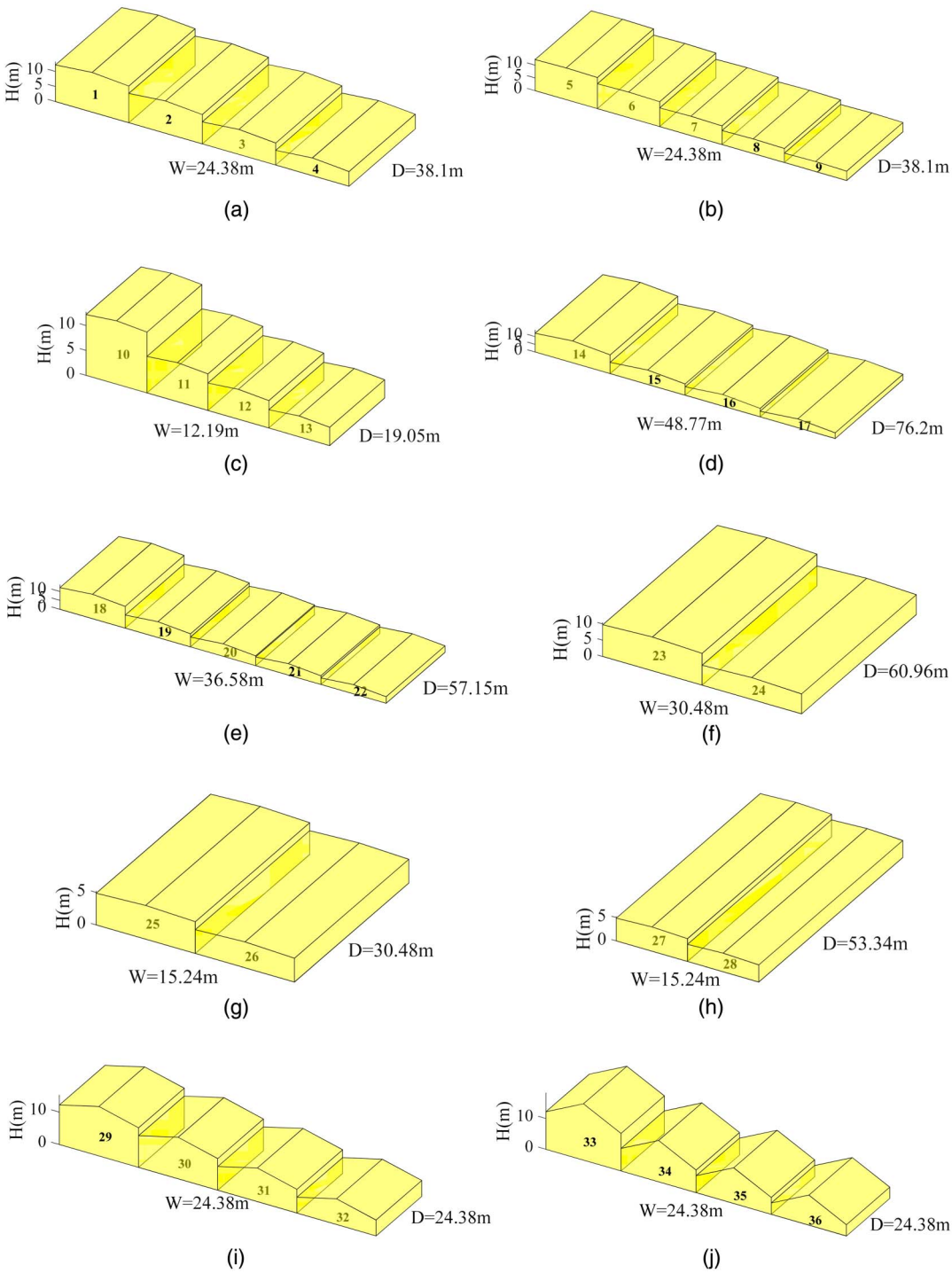

Fig. 2. Building configurations in NIST database: (a) $D = 38.1$ m, $W = 24.38$ m and roof slope = $1/12$; (b) $D = 38.1$ m, $W = 24.38$ m and roof slope = $1/48$; (c) $D = 19.05$ m, $W = 12.19$ m and roof slope = $1/12$; (d) $D = 76.2$ m, $W = 48.77$ m and roof slope = $1/12$; (e) $D = 57.15$ m, $W = 36.58$ m and roof slope = $1/12$; (f) $D = 60.96$ m, $W = 30.48$ m and roof slope = $1/24$; (g) $D = 30.48$ m, $W = 15.24$ m and roof slope = $1/24$; (h) $D = 53.34$ m, $W = 15.24$ m and roof slope = $1/24$; (i) $D = 38.1$ m, $W = 24.38$ m and roof slope = $3/12$; and (j) $D = 38.1$ m, $W = 24.38$ m and roof slope = $6/12$.

Downloaded from ascelibrary.org by University of Western Ontario on 09/05/22. Copyright ASCE. For personal use only; all rights reserved.

Methodology

Terminology

The MWFRS loads in ASCE 7-16 refer to the overall structural responses: uplift, C_u, and base shear, C_b. Neither of these loads depends on the structural system when the building is rigid—they are aerodynamic and depend only on the building shape and terrain. Here, the internal reactions are not considered, as was done in Stathopoulos (1979) or St. Pierre et al. (2005). In addition, C&C loads in Chapter 30 refer to Chapter 27 loads for effective wind areas larger than 65 m^2. Thus, area-averaged wall pressure coefficients must also be considered. The load cases in Chapter 27 are called the Directional Method because the load cases depend on the quadrant of the wind direction with respect to the building axes. In the present study, the load case for the wind directions of 0°–45° is described as parallel to roof ridge, while those from the wind directions of 45°–90° are described as normal to roof ridge, as defined in Fig. 1. These two load cases correspond to the two wind load cases in Chapter 27. Fig. 1 also defines several parameters related to the building geometry. Note that the building breadth, B, and length, L, depend on wind direction. The appropriate load case in Chapter 28 depends on the structural system, which is not considered in the current study, as noted above.

Data Sources

The primary wind tunnel data employed in the present analysis are from the National Institute of Standards and Technology (NIST) aerodynamic database, measured in Boundary Layer Wind Tunnel

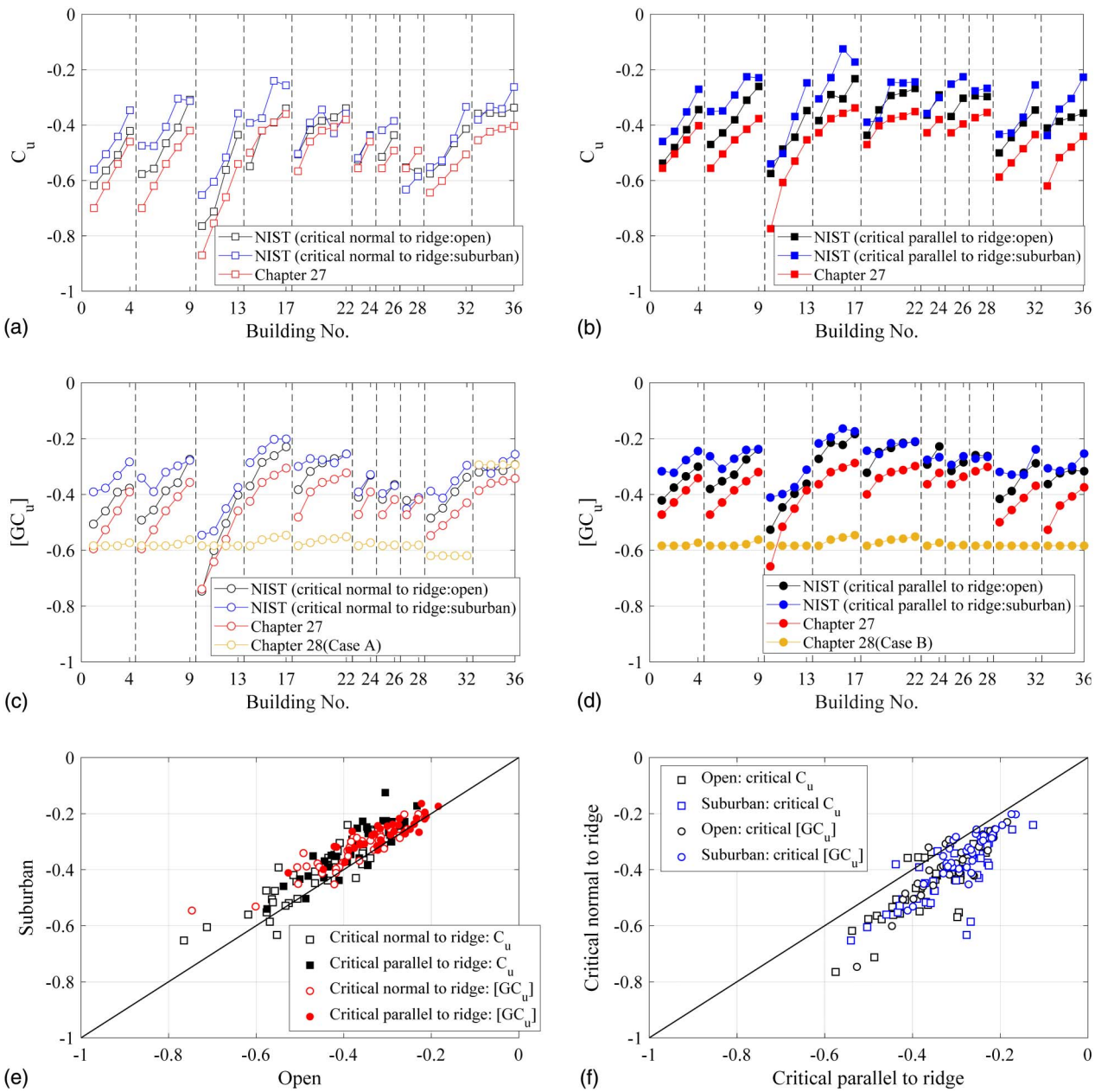

Fig. 3. Critical mean and peak uplift coefficients: (a) critical mean uplift coefficients—normal to roof ridge; (b) critical mean uplift coefficients—parallel to roof ridge; (c) critical peak uplift coefficients—normal to roof ridge; (d) critical peak uplift coefficients—parallel to roof ridge; (e) critical mean and peak uplift coefficients for open country versus those for suburban exposure; and (f) critical mean and peak uplift coefficients for normal-to-roof-ridge winds versus those for parallel-to-roof-ridge winds.

Downloaded from ascelibrary.org by University of Western Ontario on 09/05/22. Copyright ASCE. For personal use only; all rights reserved.

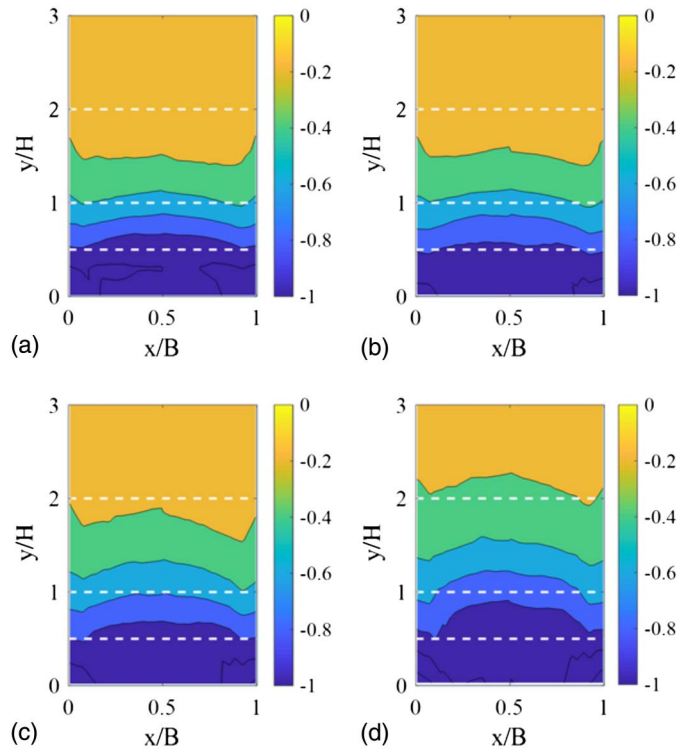

Fig. 4. Contour plot of mean pressure coefficients for building models 1–4 with roof slope of $1/12$ for the parallel-to-roof-ridge wind (white dashed line is the suggested zone boundary in Chapter 27): (a) open country, $H/L = 0.32$; (b) open country, $H/L = 0.26$; (c) open country, $H/L = 0.19$; and (d) open country, $H/L = 0.13$.

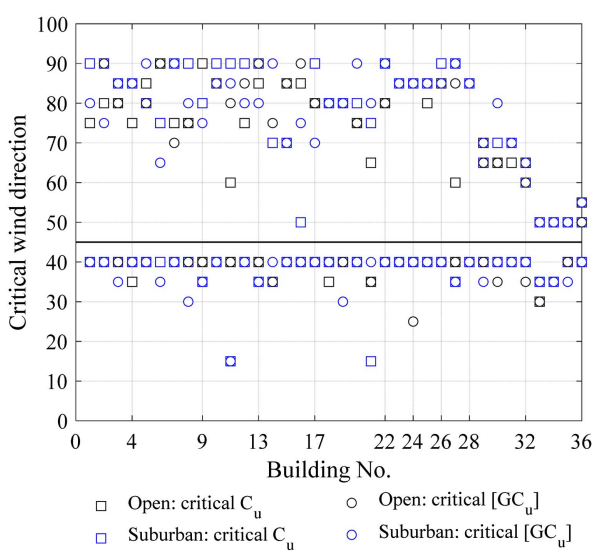

Fig. 5. Wind directions for critical mean and peak uplift coefficients.

II at the University of Western Ontario (UWO) (Ho et al. 2005). All the models were tested in two terrains, matching open country and suburban terrains prevalent in current design standards. The measured local turbulence intensities were matched closely with those in the Engineering Sciences Data Unit (ESDU 1982, 1983) for the roughness lengths (z_0) of 0.03 and 0.3 m for the open and suburban exposures, respectively, as discussed in Ho et al. (2005).

This database contains a total of 36 different building models varying in length, width, eave height, and roof slope. They can be categorized into 10 groups, with each category having the same plan dimensions and roof slope, but with varied eave heights. Nine groups of building models were measured at the length scale of $1/100$, and sampled at 500 Hz for a time period of 100 s. One group was tested at a $1/200$ length scale, with sampling rate of 400 Hz for a time period of 60 s. Ho et al. (2005) and St. Pierre et al. (2005) stated that the velocity scale in the database is assumed as being approximately 1:4, which indicates the full scale sampling frequency of approximately 20 and 16 Hz for the scales of $1/100$ and $1/200$, respectively. The output of the database is a set of pressure time series from each tap location, referenced to the dynamic velocity pressure measured at a higher level in the wind tunnel where the flow is uniform with low turbulence level. Therefore, all the data need to be re-referenced to the mean roof height dynamic pressure by the ratio of dynamic pressure at upper level and the dynamic pressure at mean roof height. Further details regarding the experimental setup and wind tunnel measurements, such as the pressure tap layout and wind simulation, can be found in the set of papers by Ho et al. (2005), St. Pierre et al. (2005), and Oh et al. (2007). The building model configurations and model numbers referred to in the NIST database are summarized in Table 1 and illustrated in Fig. 2.

It should be mentioned that two of these configurations, totaling eight building models, have already been examined by St. Pierre et al. (2005) and compared with the ASCE 7-02 provisions, which are equivalent to Chapter 28 in ASCE 7-16 for the present purposes.

Comparisons between Wind Tunnel Data and ASCE 7-16

An approach to obtain the equivalent pressure coefficients was proposed by St. Pierre et al. (2005). The precondition to use the method in St. Pierre et al. (2005) is a match between the measured wind field and ESDU model. Ho et al. (2005) presented data that indicated that the wind speed and turbulence intensity profiles for the open country match well with the ESDU model. However, the suburban terrain does not perfectly match the ESDU model for $z_o = 0.3$ m, especially for the data close to the ground. Therefore, we propose to calculate the peak pressure coefficients, $[GCp]$, by directly using the measured wind field data and neglecting the mismatch with the ESDU model such that

$$[GCp] = \frac{\hat{P}}{\bar{P}} \times \frac{1}{(1 + gI_V)^2} \times Cp \tag{2}$$

where $\hat{P}$ = peak wind pressure, which is the median value of Type I extreme value distribution that is estimated using the Lieblein BLUE formulation (Lieblein 1976); $\bar{P}$ = time-averaged wind pressure; Cp = mean pressure coefficient referenced to the mean roof height velocity; g = peak factor, which is assumed to be 3.0 in the present study (to obtain 3-s gust speeds); and I_V = turbulence intensity at mean roof height. Note that in the present paper we use C_u and $[GC_u]$ to represent the overall mean and peak uplift coefficients, and C_b and $[GC_b]$ to denote the mean and peak base shear coefficients, respectively. For the wall pressures, we employ the consistent symbols, Cp and $[GCp]$, as in ASCE 7-16.

In the present paper, vertical uplift is simply the vertical component of the wind loading acting on the roof area. Base shear is the net horizontal force acting on opposite vertical planes of the structure as indicated by the coordinate system in Fig. 1, including the vertical projection of the roof when the roof slope is greater than

Downloaded from ascelibrary.org by University of Western Ontario on 09/05/22. Copyright ASCE. For personal use only; all rights reserved.

10°. The readers can refer to Appendix A in St. Pierre et al. (2005) for the calculation methods of these structural load coefficients.

Area-Averaged Pressure Coefficients

Overall Load Coefficients

Uplift

Figs. 3(a–d) present the mean, C_u, and peak, $[GC_u]$, uplift coefficients as a function of building configuration. Note that the building numbers in Fig. 3 correspond to those in Table 1 and Fig. 2. The dark vertical dashed lines in Figs. 3(a–d) denote the building groups, and the data in each group are intended to illustrate the trend of uplift with building configuration. It should be noted that the structural loads from Chapter 28 are the worst case for the two directions of MWFRS being designed. A significant increase in the uplift with roof height, H, is observed for all buildings, consistent with the findings in St. Pierre et al. (2005), even though only the bay force was considered in their paper. It can be seen that Chapter 27 can reasonably and conservatively evaluate the mean overall uplift. In addition, it is clear that the pressure coefficients depend on

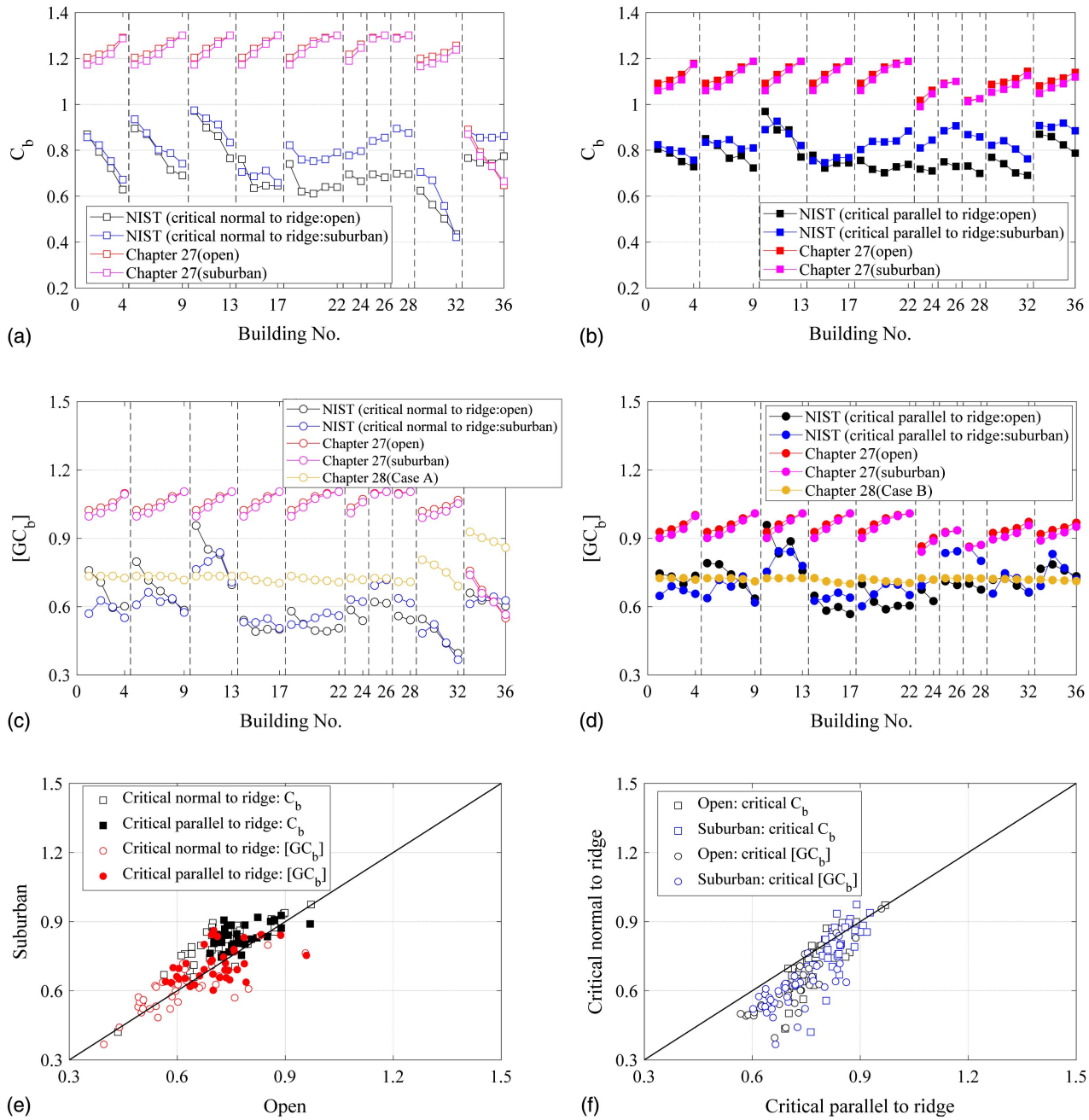

Fig. 6. Critical mean and peak base shear coefficients: (a) critical mean base shear coefficients—normal to roof ridge; (b) critical mean base shear coefficients—parallel to roof ridge; (c) critical peak base shear coefficients—normal to roof ridge; (d) critical peak base shear coefficients—parallel to roof ridge; (e) critical mean and peak base shear coefficients for suburban exposure versus those for open country; and (f) critical mean and peak base shear coefficients for normal-to-roof-ridge winds versus those for parallel-to-roof-ridge winds.

Downloaded from ascelibrary.org by University of Western Ontario on 09/05/22. Copyright ASCE. For personal use only; all rights reserved.

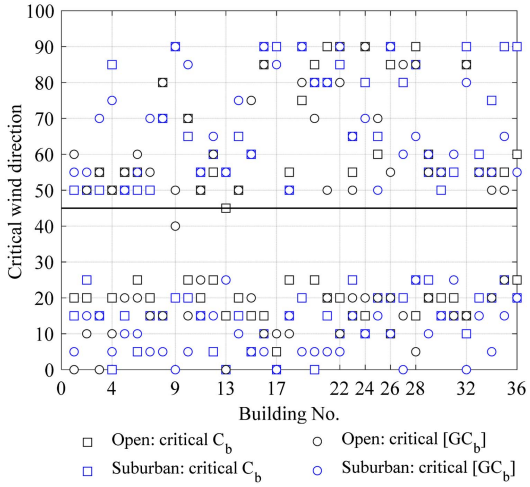

Fig. 7. Critical wind directions for base shear.

building geometry; thus, Chapter 28 cannot capture these variations with fixed values, although it does envelop most of the building configurations conservatively.

The uplift coefficients for the open country versus suburban terrain are presented in Fig. 3(e). The dark solid line with slope of 1:1 is used to illustrate how similar or different the coefficients are. The data indicate that the mean and peak uplift coefficients for suburban terrain are similar to the open exposure, consistent with the findings of Wu and Kopp (2018) and the assumption of ASCE 7-16 that the building aerodynamics do not vary with terrain. In addition, it can be seen that the critical normal-to-ridge winds generate higher uplift than the critical parallel-to-ridge winds, as shown in Fig. 3(f). This is because the flow reattachment length is approximately equal to H (Akon and Kopp 2016) and complete pressure recovery occurs for approximately $1.5H$, for typical open country and suburban terrains. Therefore, the larger length, L, generates a lower uplift coefficient for the ridge direction and plan aspect ratios considered in this database.

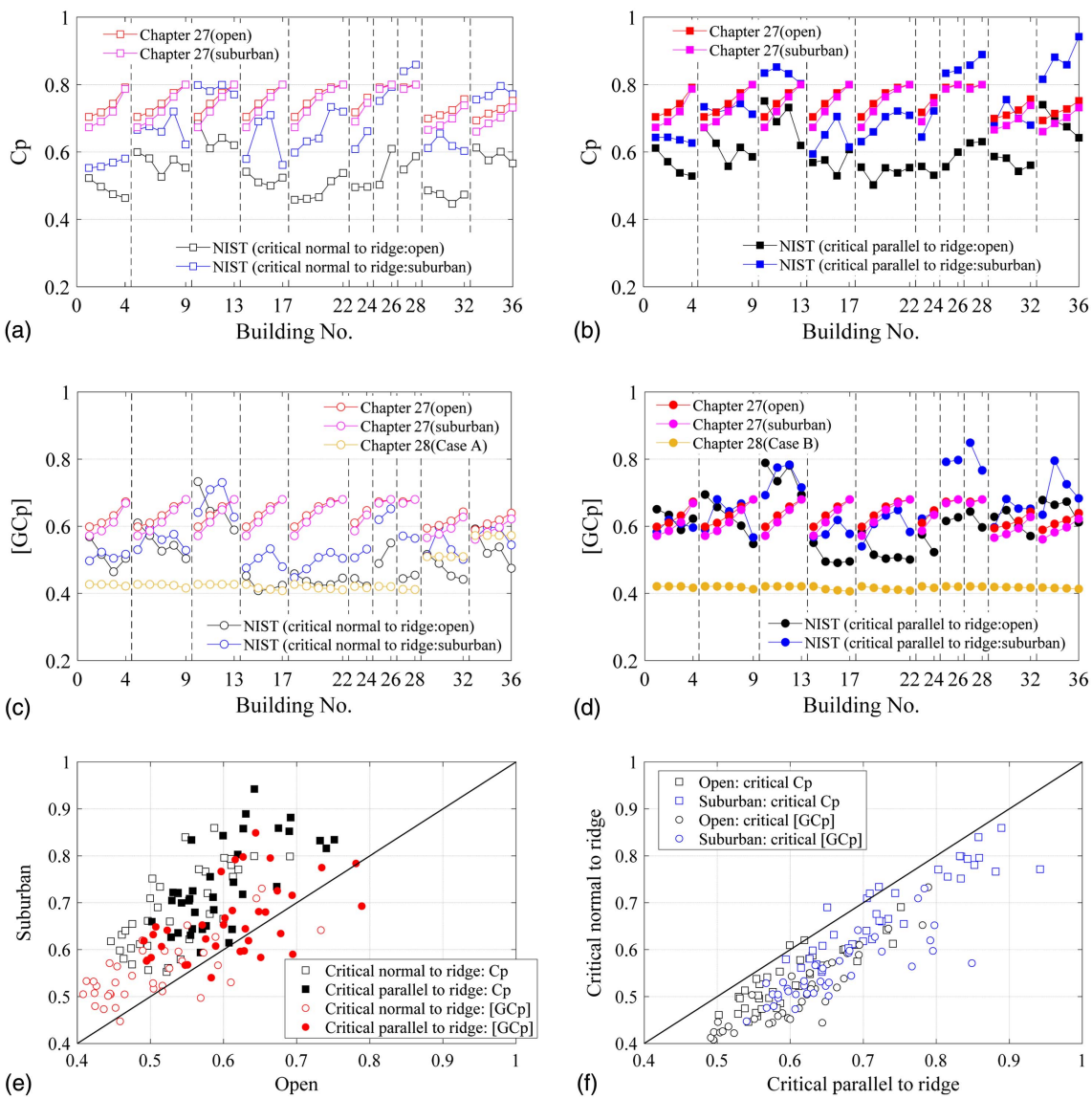

Fig. 8. Critical mean and peak area-averaged windward wall pressure coefficients: (a) critical mean pressure coefficients—normal to roof ridge; (b) critical mean pressure coefficients—parallel to roof ridge; (c) critical peak pressure coefficients—normal to roof ridge; (d) critical peak pressure coefficients—parallel to roof ridge; (e) critical mean and peak pressure coefficients for open exposure versus those for suburban cases; and (f) critical mean and peak pressure coefficients for normal-to-roof-ridge winds versus those for parallel-to-roof-ridge winds.

Downloaded from ascelibrary.org by University of Western Ontario on 09/05/22. Copyright ASCE. For personal use only; all rights reserved.

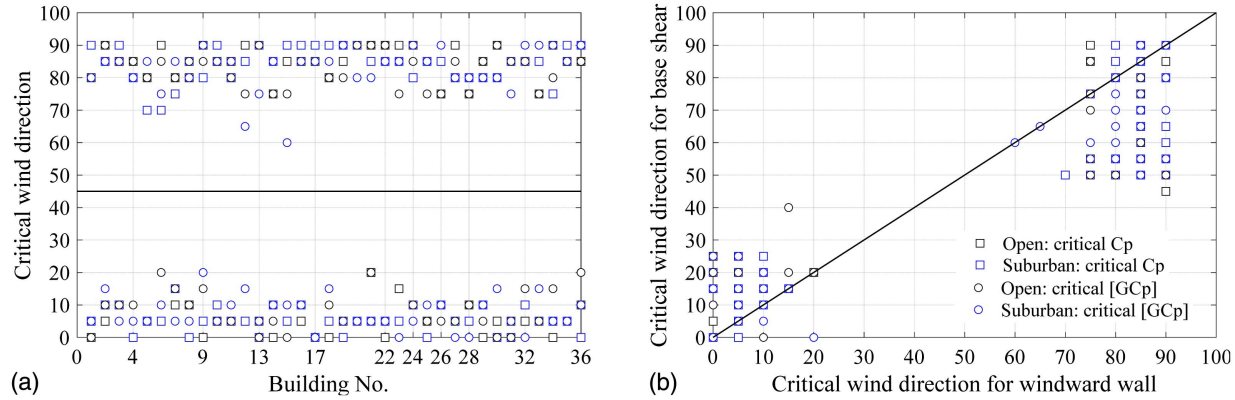

Fig. 9. Critical wind direction for windward wall pressure coefficients: (a) critical wind direction for windward wall pressure coefficients versus building configurations; and (b) critical wind directions for base shears versus those for windward wall pressures.

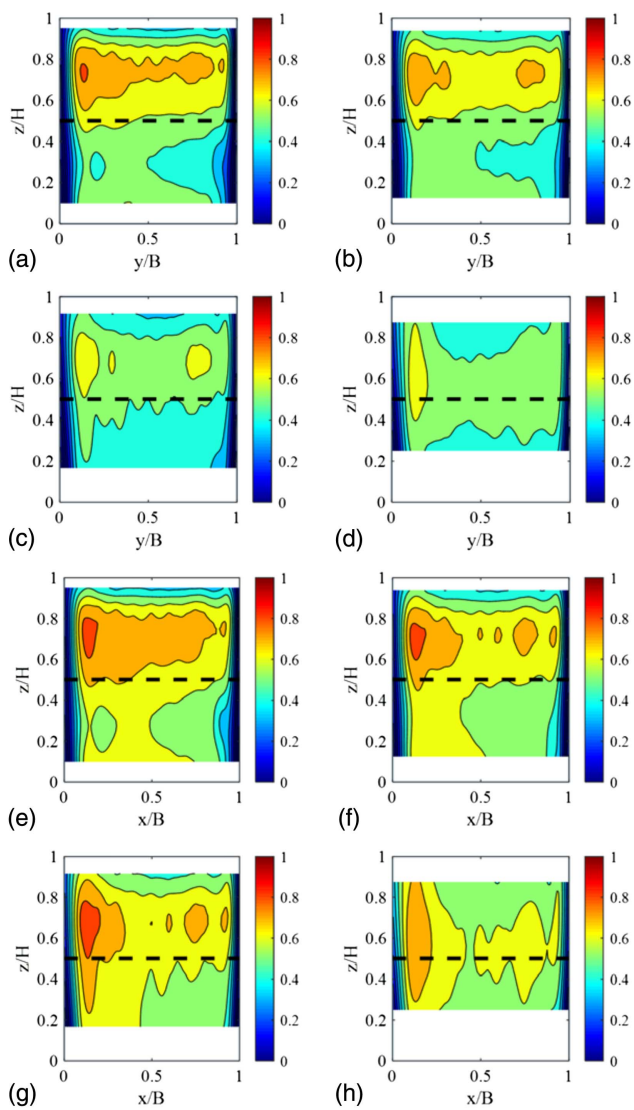

Fig. 10. Contour plot of mean pressure coefficients for building models 1–4 for the normal-to-roof-ridge winds (black dashed line is the suggested zone bound): (a) open country, $H/B = 0.32$; (b) open country, $H/B = 0.26$; (c) open country, $H/B = 0.19$; (d) open country, $H/B = 0.13$; (e) suburban terrain, $H/B = 0.32$; (f) suburban terrain, $H/B = 0.26$; (g) suburban terrain, $H/B = 0.19$; and (h) suburban terrain, $H/B = 0.13$.

Chapter 27 is able to estimate the uplift coefficients with reasonable accuracy, which indicates that the zones and zone pressure coefficients work well. This is examined in Fig. 4, which presents pressure coefficient contour plots for the roof. The distance, y, from the leading edge is normalized by roof height, H. Note that the plotting area is confined to $y/H = 3$, for the four buildings, to make the illustrations legible. The white dashed line denotes the zone boundary given by the provisions of Chapter 27. Clearly, the zones given in Chapter 27 are reasonable, although not perfect, with the ratio, H/L, being the critical geometric parameter.

Fig. 5 shows the critical wind directions for the mean and peak uplift coefficients in Fig. 3. Note that two critical wind directions—i.e., critical parallel to ridge and normal to ridge—are presented. The solid dark line in Fig. 5 is for the wind direction of 45°, indicating the boundary between the critical parallel-to-ridge winds and critical normal-to-ridge winds. The observations and findings can be summarized as follows. First, the critical wind directions for open country and suburban terrain are similar for the critical parallel-to-ridge case, as are the critical wind directions for mean and peak uplift coefficient. For the critical normal-to-ridge wind directions, the values for open country and suburban terrain are more scattered, but a similar tendency with roof slope is observed for both the open and suburban exposures. Second, the wind directions for the critical normal-to-ridge winds depend on the roof slope. The wind directions range from 70° to 90° for buildings with roof slopes smaller than 10°, while winds from 60° to 70° cause the worst wind loads on buildings with a roof slope of 14°, and winds of 50°–60° generate the worst wind loads on buildings with a roof slope of 27°. Third, wind directions of approximately 40° are responsible for the worst parallel-to-ridge case, due to the conical vortex, for most building configurations.

Base Shear

Fig. 6 presents the critical mean and peak base shear coefficients, C_b and $[GC_b]$, respectively. Since the velocity pressure factor, K_H, varies with terrain classification, two sets of base shear coefficients from Chapter 27 are shown in Fig. 6. Note that the trend of the provisions in Chapter 27 with building geometry is due to the transformation factor, F_c, expressed by Eq. (1). Several observations can be made. First, the dependence of base shear on roof height is not accurately captured by the ASCE 7-16 provisions. As for the uplift coefficients, Chapter 28 does not capture the geometric tendencies with fixed values for base shear. In general, the Chapter 27 provisions are considerably more conservative than those in Chapter 28. Second, the mean base shears for open country are similar to

Downloaded from ascelibrary.org by University of Western Ontario on 09/05/22. Copyright ASCE. For personal use only; all rights reserved.

those for suburban terrain for Building No. 1–17. For the buildings with large plan dimensions (No. 18–28) and high roof slopes (No. 29–36), the open country coefficients are distinctly smaller than the base shear coefficients for the suburban exposure. Third, the peak base shear coefficients for open country follow the same trend with roof height as do the mean values. However, this is not distinctly observed for the suburban exposure, possibly due to the turbulence intensity uncertainties for the suburban terrain (Ho et al. 2005). Fourth, the variation of mean base shear with roof height for open country is inconspicuous for buildings with large plan dimensions. Fifth, the normal-to-ridge load case in Chapter 27 approaches the wind tunnel data for the buildings with a roof slope of 27° for both mean and peak base shear coefficients. Sixth, Fig. 6(e) shows that the mean base shear coefficients for open country tend to be slightly smaller than those for suburban exposure. The open country values are lower than the peak base shear for suburban terrain for most building configurations, except for the buildings with a roof height of 12.19 m. Last, base shear coefficients observed for the parallel-to-ridge winds are higher than those for the normal-to-ridge winds. These observations from Fig. 6 imply that the wall pressure coefficients depend on roof height, which contrasts with the provisions of Chapter 27. Further detailed discussion on the wall pressure coefficients will be presented in the following sections.

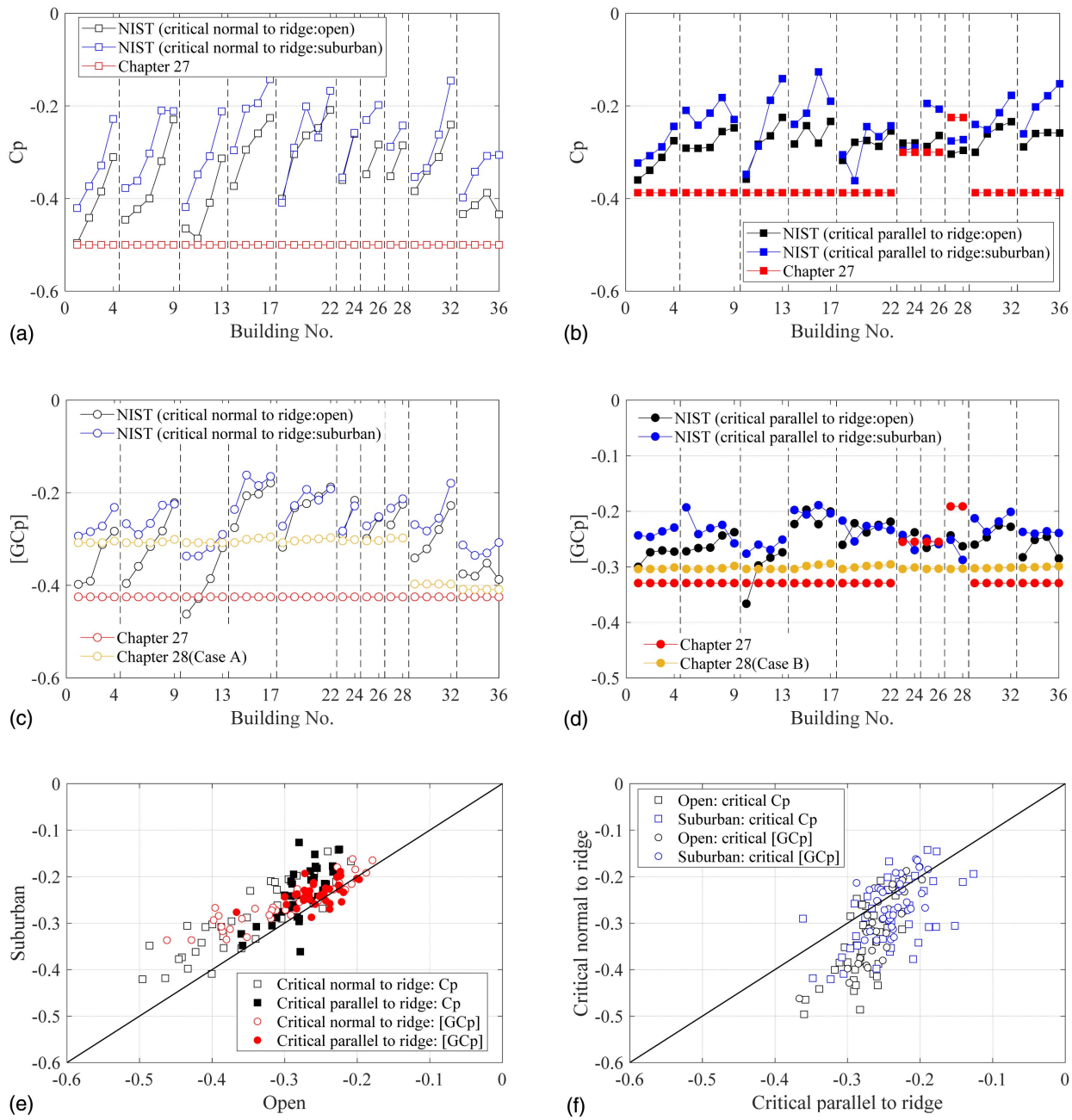

Fig. 11. Critical mean and peak area-averaged leeward wall pressure coefficients: (a) critical mean pressure coefficients—normal to roof ridge; (b) critical mean pressure coefficients—parallel to roof ridge; (c) critical peak pressure coefficients—normal to roof ridge; (d) critical peak pressure coefficients—parallel to roof ridge; (e) critical mean and peak pressure coefficients for open exposure versus those for suburban cases; and (f) critical mean and peak pressure coefficients for normal-to-roof-ridge winds versus those for parallel-to-roof-ridge winds.

Downloaded from ascelibrary.org by University of Western Ontario on 09/05/22. Copyright ASCE. For personal use only; all rights reserved.

Fig. 7 shows the wind directions for the critical mean and peak base shear coefficients. As for the uplift, the critical parallel-to-ridge wind directions for open country are similar to those for suburban terrain, and the wind directions for the critical mean and peak base shears are also close. The wind directions for the critical parallel-to-ridge wind loads are in the range of 0°–30°, while they vary over a larger range of 50°–90° for the critical normal-to-ridge wind loads. It is also worthwhile to note that the peak base shear does not occur for the same wind directions as the peak uplift. The roles of windward wall and leeward wall pressures on the base shears will be discussed in the following sections.

Area-Averaged Wall Pressure Coefficients

Windward Walls

Fig. 8 shows the critical mean and peak area-averaged windward wall pressure coefficients versus building configuration. [Note that the values of Chapter 27 were re-referenced to the roof height wind velocity using Eq. (1)] As for the base shear, two sets of windward wall pressure coefficients from Chapter 27 are provided. The observations for windward walls are consistent with those for base shears, and for the sake of brevity, we will not repeat the findings here. It is worth emphasizing that the peak area-averaged wall pressure coefficients show tendencies with roof height for open country; however, these are not distinctly observed for suburban terrain. In addition, the mean values for both open country and suburban terrain seem more scattered than the peak values, possibly due to the measurement uncertainty (Diaz 2006). Peak values for open country deviate from those for suburban terrain, but the differences are not as significant as for the mean values. Chapter 28 significantly underestimates the measured peak values.

Fig. 9(a) shows the wind directions for critical mean and peak windward wall pressure coefficients versus building configurations, and Fig. 9(b) presents how the critical wind directions for base shear are similar or different with those for windward wall pressures. The critical normal-to-ridge winds of 70°–90° and critical parallel-to-ridge winds of 0°–20° are observed. It can be observed that the wind directions for critical windward wall pressures are scattered around those for critical base shear coefficients, as seen in Fig. 9(b). The predominant contribution of windward wall and leeward wall pressures on base shear will be further elaborated in the next section for leeward wall.

Contour plots of mean windward wall pressure coefficients for open country and suburban terrain are presented in Fig. 10. These pressure distributions show that the mean coefficients increase with H/B. A greater pressure tap resolution would help to resolve some of the differences in the patterns and scatter in the mean values. Hong (2017) observed that the individual peak pressures increase with H/B but remain constant for about $H/B > 1$, without considering the area-averaged wall pressure coefficients. This pattern of mean windward wall pressures is similar to that found in Hong's study.

Leeward Walls

Fig. 11 shows the critical mean and peak area-averaged leeward wall pressure coefficients. Several observations from Fig. 11 can be made. First, the provisions of Chapter 27 envelop the mean and most of the peak leeward wall pressures, but underestimate the peak values for a few buildings with small plan dimensions. Chapter 28 underestimates the peak leeward wall pressures for the buildings with the larger roof heights. Second, both Chapter 27, which specifies the pressure coefficients as a function of L/B, and Chapter 28, with almost fixed values, do not capture the trends of the leeward wall pressure coefficients with roof height. The tendency with roof height is more distinct for the critical normal-to-ridge winds than for critical parallel-to-ridge winds. Third, the leeward wall pressure coefficients for suburban terrain are slightly smaller in magnitude than the mean values for open country, as shown in Fig. 11(e). Fourth, Fig. 11(f) indicates that the leeward wall pressure coefficients for critical normal-to-ridge winds tend to exceed those for critical parallel-to-ridge winds. Fig. 12 shows the contour plots for roof and leeward wall pressure coefficients, which demonstrate that the leeward walls are closely related to the pressures in the zone downstream of the reattachment on the roof. Therefore, the explanation for Fig. 11(f) is the recovery or re-separation of flow after the ridge, which increases the leeward wall magnitudes for the normal-to-ridge wind directions even when the slopes are low.

Fig. 13 presents the wind directions for critical mean and peak leeward wall pressure coefficients. The critical wind directions are mainly centered about 45°, that is, critical parallel-to-ridge wind

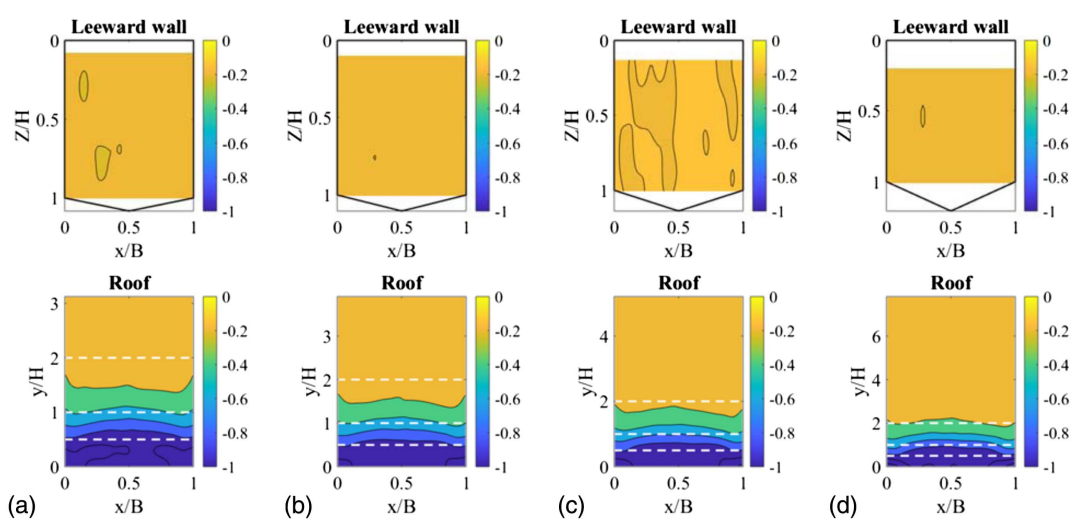

Fig. 12. Contour plots of mean pressure coefficients for building models 1–4 with roof slope of 1/12 for the parallel-to-roof-ridge wind (white dashed line is the suggested zone boundary for uplift in Chapter 27): (a) open country, $H/L = 0.32$; (b) open country, $H/L = 0.26$; (c) open country, $H/L = 0.19$; and (d) open country, $H/L = 0.13$.

Downloaded from ascelibrary.org by University of Western Ontario on 09/05/22. Copyright ASCE. For personal use only; all rights reserved.

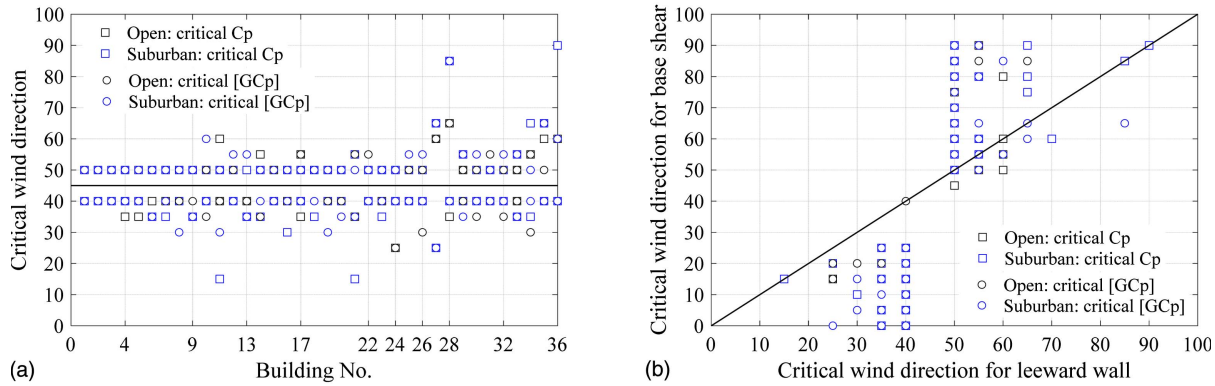

Fig. 13. Critical wind direction for leeward wall pressure coefficients: (a) critical wind direction for leeward wall pressure coefficients versus building configurations; and (b) critical wind directions for base shears versus those for leeward wall pressures.

directions of 40° and critical normal-to-ridge wind directions of 50°. Both the wind directions for critical parallel-to-ridge and normal-to-ridge deviate from the critical wind directions for base shear. Fig. 14 further presents the critical windward and leeward wall pressures versus critical base shear coefficients. The dark solid line indicates that the wall pressures are most closely related to the base shear, which indicates that design loads would be easier to model based on the windward wall pressures than on the leeward walls.

Side Walls

The worst side wall pressure coefficients are presented in Fig. 15. These tend to be the more leeward of the two side walls. Note that Chapter 28 does not provide the side wall pressure coefficients for Case A; therefore, only Case B is given in Figs. 15(c and d). It can be observed that the mean value of −0.7 in Chapter 27 is greater in magnitude than the NIST data. In addition, Chapters 27 and 28 do not accurately evaluate the peak side wall pressure coefficient variations with building geometry because they are constant with building geometry, while the measured data have clear trends. The figure shows that the magnitude of the side wall pressure coefficients increase with roof height for the critical parallel-to-ridge wind direction, just as for the uplift coefficients. For the critical normal-to-ridge wind directions, the same trend with roof height is observed, except for the buildings with a roof slope of 27° (No. 33–36). Similarly, the open country can represent the mean pressure coefficients for other surface terrains, as shown in Fig. 15(e). The normal-to-ridge winds would create higher negative pressures on the side walls compared with the parallel-to-ridge winds, as shown in Fig. 15(f). It is observed that the side wall pressure coefficients are linearly related to the uplift coefficients, as shown in Fig. 15(g). It should be noted that the only significant deviations between side wall pressure coefficients and uplift coefficients are for the buildings with high-slope roof, as emphasized by data in the circle. Fig. 16 presents the contour plots for roof and

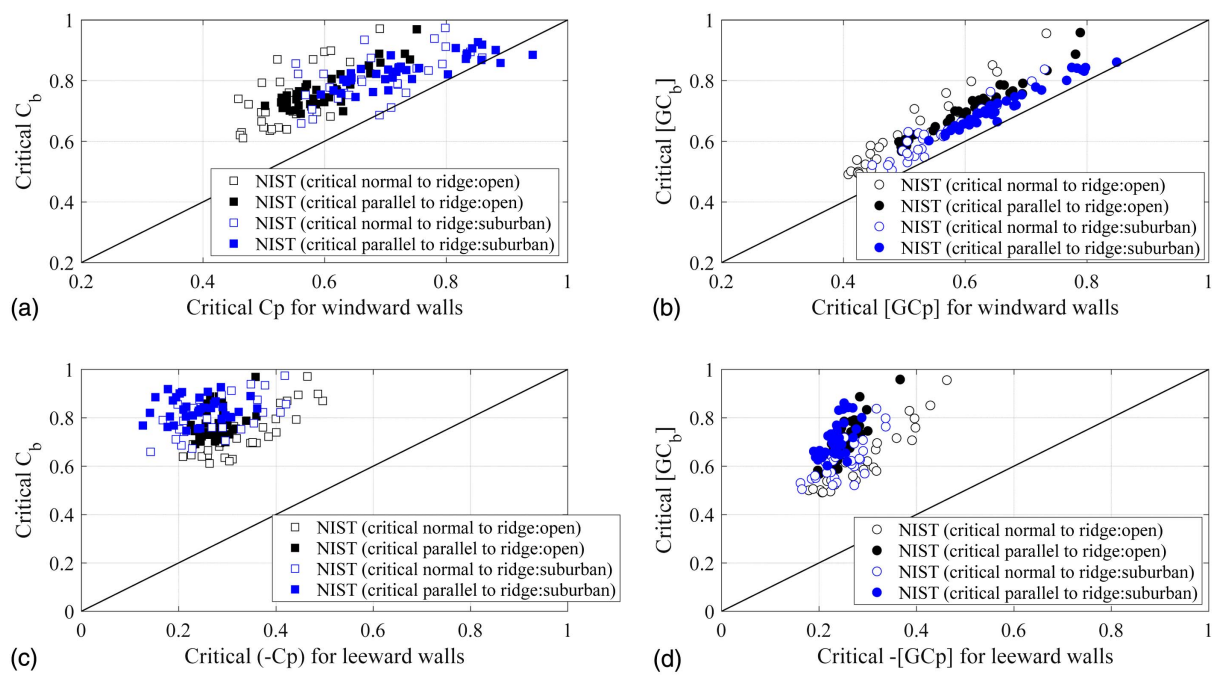

Fig. 14. Critical windward and leeward wall pressure coefficients versus critical base shear coefficients: (a) critical mean windward wall pressures versus critical mean base shear; (b) critical peak windward wall pressures versus critical peak base shear; (c) critical mean leeward wall pressures versus critical mean base shear; and (d) critical peak leeward wall pressures versus critical peak base shear.

Downloaded from ascelibrary.org by University of Western Ontario on 09/05/22. Copyright ASCE. For personal use only; all rights reserved.

Downloaded from ascelibrary.org by University of Western Ontario on 09/05/22. Copyright ASCE. For personal use only; all rights reserved.

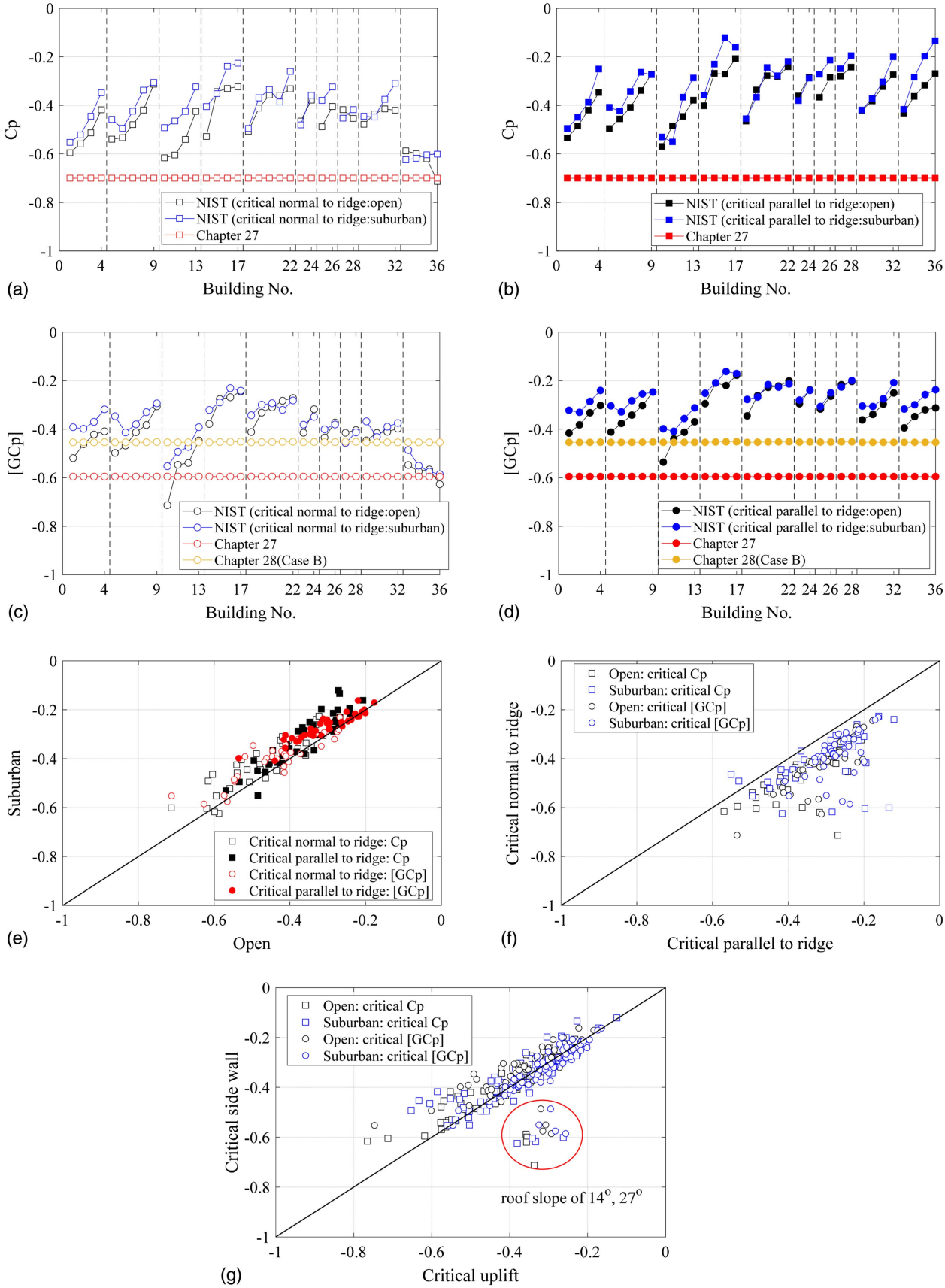

Fig. 15. Critical mean and peak area-averaged side wall pressure coefficients: (a) critical mean pressure coefficients—normal to roof ridge; (b) critical mean pressure coefficients—parallel to roof ridge; (c) critical peak pressure coefficients—normal to roof ridge; (d) critical peak pressure coefficients—parallel to roof ridge; (e) critical mean and peak pressure coefficients for open exposure versus suburban cases; (f) critical mean and peak pressure coefficients for normal-to-roof-ridge winds versus parallel-to-roof-ridge winds; and (g) critical uplift coefficients versus critical side wall pressure coefficients.

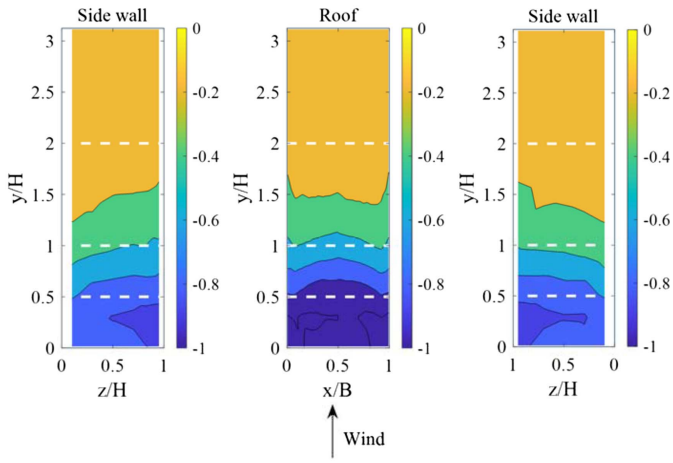

Fig. 16. Contour plots of the mean pressure coefficients for the buildings with $H = 12.19$ m, $D = 38.1$ m, $W = 24.38$ m, and roof slope of $1/12$ (the white dashed line denotes the zone boundary provided in Chapter 27).

side walls, and the white lines denote the critical boundaries for uplift provided in Chapter 27, which further proves the similarity between side wall and roof pressures.

Fig. 17 shows the wind directions for the critical mean and peak side wall pressure coefficients, and the comparisons with those for critical uplift coefficients. The critical parallel-to-ridge wind directions are confined within the range of 20°–40°, which are wider than those for critical uplifts. In addition, the critical normal-to-ridge wind directions are mainly in the range of 70°–90°.

Summary

Aerodynamic data for 36 low-rise building shapes have been compared to the provisions in Chapters 27 and 28 of ASCE 7-16. In particular, overall building uplift and base shear, along with the windward, leeward, and side wall area-averaged pressure coefficients have been examined. For uplift, the Chapter 27 provisions depend on H/L, which works well at capturing the functional variations and the load levels. The constant values of Chapter 28 do not capture these functional variations but envelop the data for the many, but not all, of the buildings. For base shear, Chapter 27 does not capture the variations of the load coefficients, which tend to increase with building height. For Chapter 28, with constant values, neither the functional variations with building geometry nor the magnitude of the load coefficients follows the data, although it is reasonable for the lowest buildings, building with very large plan dimensions, and for loads normal-to-ridge with larger roof slopes. In the next section, we examine further the geometric parameters that control the wind loads.

Effects of Building Geometry

As shown in the previous sections, the measurements indicate that the roof height, H, plays a significant role on the wind loads on low-rise buildings. However, other geometric parameters also play a role. The provisions of Chapter 27 are able to partially capture these, while Chapter 28, with its fixed pressure coefficients, tends not to. The purpose of this section is to examine the roles of the primary geometric parameters (H, L, B) on mean and peak loads for low-slope roofs (i.e., roof slopes smaller than 10°). The approach here is to examine nondimensional parameters of the building parameters (i.e., H/L, H/B, and L/B) to determine if any of these can collapse the data reasonably well. For example, the mismatch in the base shear between the measured data and Chapter 27, where the pressure coefficients depend on L/B for the same roof height, suggests that L/B may not be the best parameter for codifying the wall pressure coefficients. Such details are examined in this section.

Uplift

Fig. 18 presents the critical mean and peak uplift coefficients as functions of H/L, H/B, and L/B. There are two separate trend lines for the data plotted versus H/B corresponding to the two critical load cases, as shown in Figs. 18(c and d). The scattered points in Figs. 18(e and f) further illustrate the lack of functional dependence on the plan dimension aspect ratio, L/B. The monotonic tendency of uplift with H/L in the wind tunnel data is consistent with the tabulated values in Chapter 27, indicating that H/L is the most accurate parameter to determine the uplift. Chapter 27 envelops the critical mean uplift coefficients and captures the critical peak uplift coefficients. As discussed in the previous section, Chapter 28 cannot capture the trend of increasing uplift with H/L, given those fixed coefficients. In addition, Chapter 28 begins to underestimate the uplift on the buildings with $H/L > 0.6$, but overestimates the uplift for $H/L < 0.4$, especially for the limit case of H/L approaching 0.

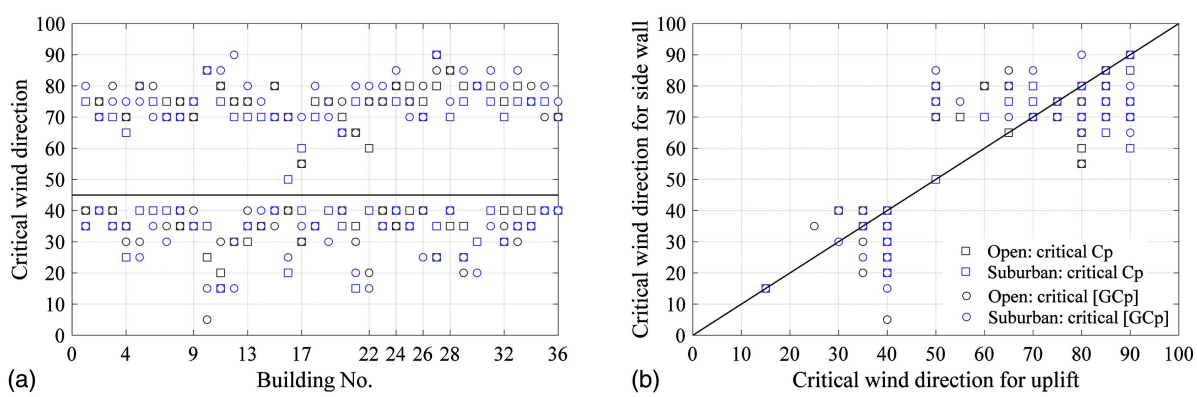

Fig. 17. Critical wind directions for side wall pressure coefficients: (a) critical wind directions for side wall pressure coefficients versus building configurations; and (b) critical wind directions for side wall pressures versus those for uplift.

Downloaded from ascelibrary.org by University of Western Ontario on 09/05/22. Copyright ASCE. For personal use only; all rights reserved.

Downloaded from ascelibrary.org by University of Western Ontario on 09/05/22. Copyright ASCE. For personal use only; all rights reserved.

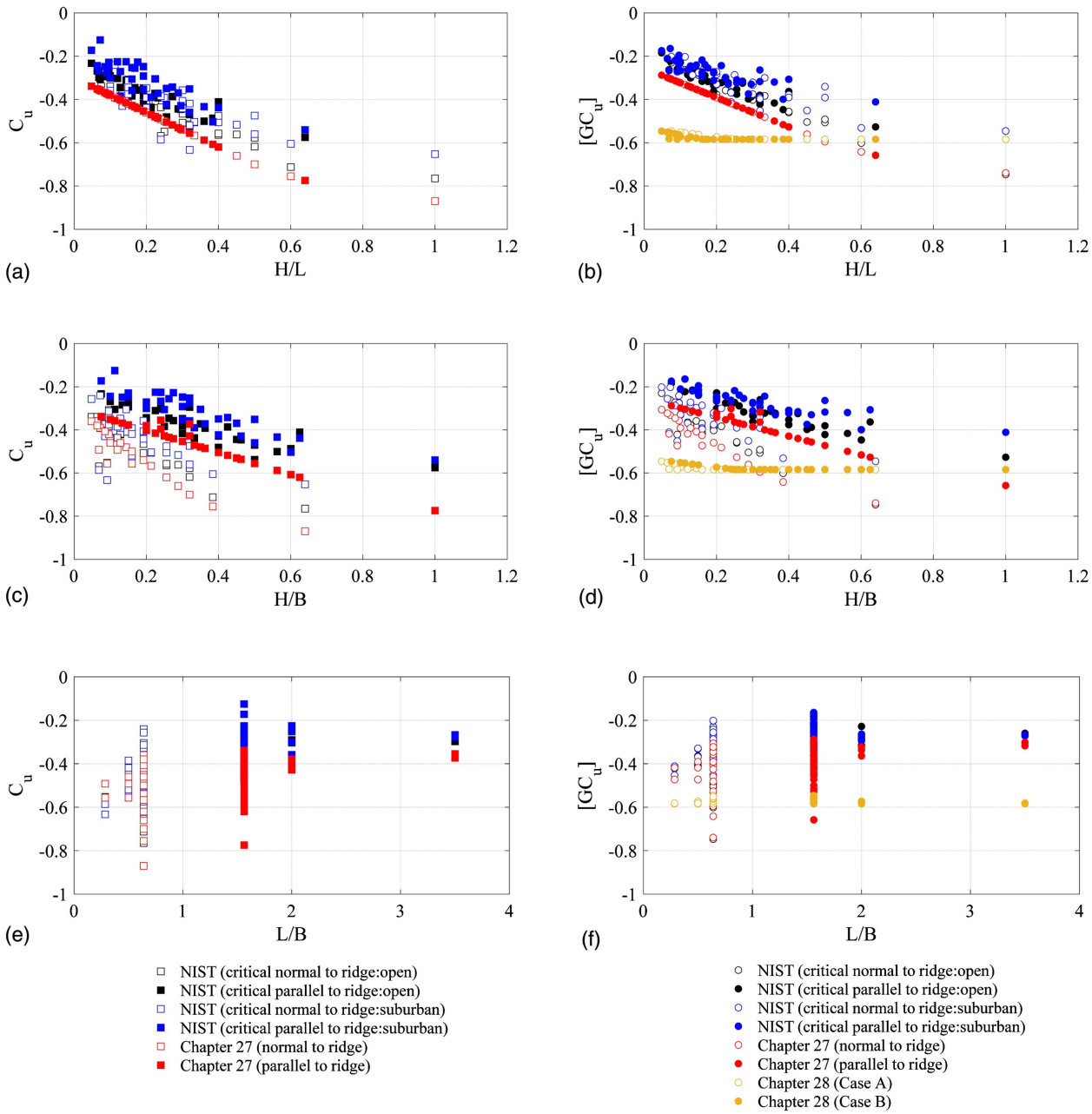

Fig. 18. Critical mean and peak uplift coefficients versus H/L, H/B, and L/B: (a) critical mean pressure coefficients versus H/L; (b) critical peak pressure coefficients versus H/L; (c) critical mean pressure coefficients versus H/B; (d) critical peak pressure coefficients versus H/B; (e) critical mean pressure coefficients versus L/B; and (f) critical peak pressure coefficients versus L/B.

Side Walls

Fig. 19 provides the dependence of side wall pressure coefficients on the same nondimensional geometric parameters. Earlier, Figs. 15 and 16 demonstrated similarity between the side wall and roof pressures. Thus, the provisions for uplift in Chapter 27 are also presented as the light square and light circle markers in Figs. 19(a and b). It can be seen that L/B and H/B are less accurate in modeling the side wall pressure coefficients for low-rise buildings. The side wall pressure coefficients decrease (i.e., are more negative) with H/L. These results indicate that, if the roof provisions were to be applied to the side walls, they would be more economical than the current provisions, which have fixed values. In addition, Chapter 28 provides nonconservative design wind loads when $H/L > 0.5$, but works well for the lower roof heights or larger plan dimensions.

Windward Walls

Fig. 20 depicts the critical windward wall pressure coefficients versus the three nondimensional parameters, H/L, H/B, and L/B. In addition, they are also plotted relative to the roof height, H (as in the provisions of Chapter 27). Several observations can be made. First, both the critical mean and peak windward wall pressure coefficients are scattered versus roof height, H, even though Fig. 11 shows variations with roof height for the open country terrain. The provisions in Chapter 27 tend to constant values of 0.66 for mean and 0.56 for peak, when $H > 15$ m. Second, the critical windward wall pressure coefficients are scattered versus the parameters of H/L and L/B. However, the peak coefficients exhibit some tendency to increase with H/B for the open country terrain. The windward wall pressure distribution for suburban terrain shows a less

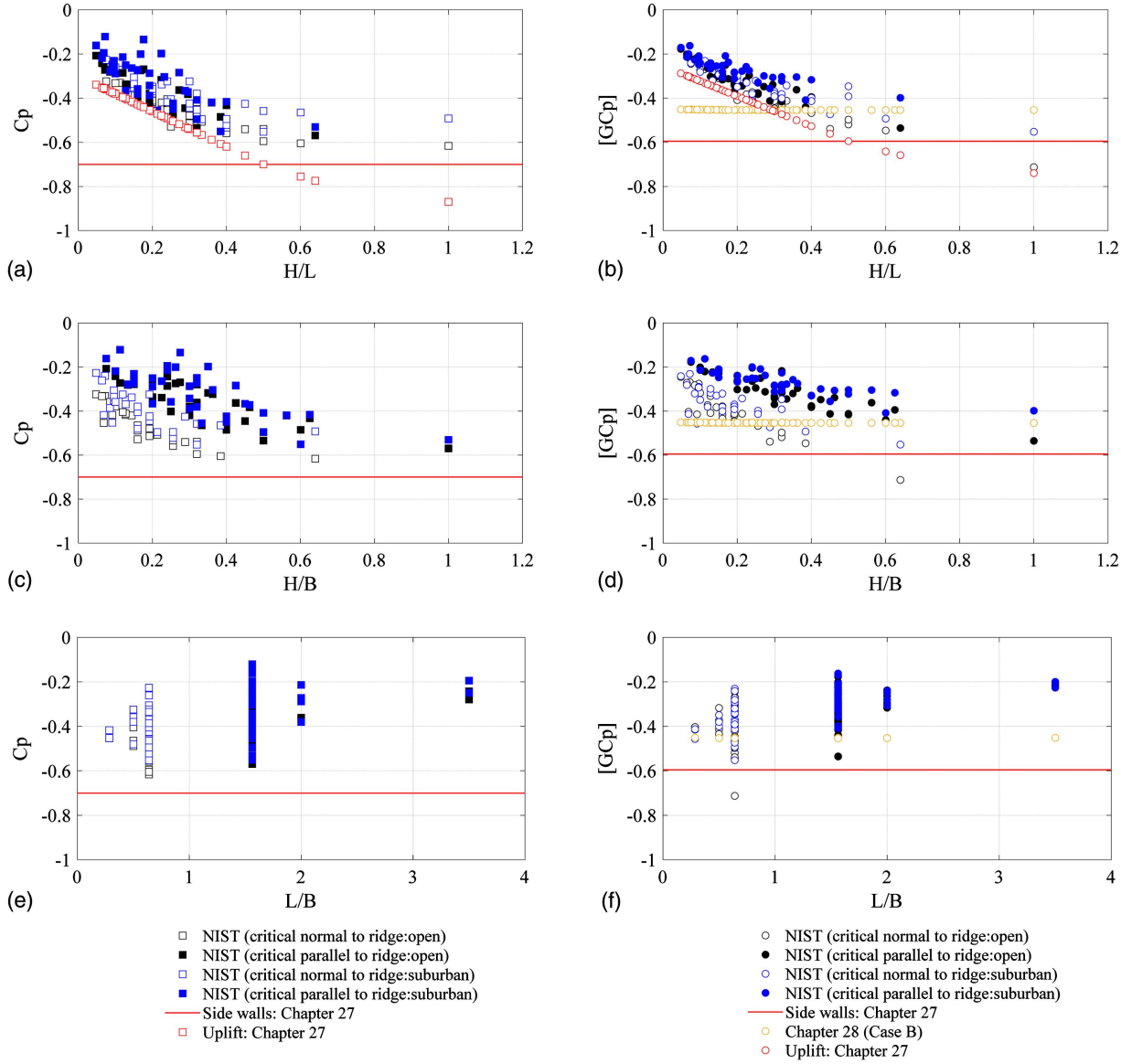

Fig. 19. Critical mean and peak side wall pressure coefficients versus H/L, H/B, and L/B: (a) critical mean pressure coefficients versus H/L; (b) critical peak pressure coefficients versus H/L; (c) critical mean pressure coefficients versus H/B; (d) critical peak pressure coefficients versus H/B; (e) critical mean pressure coefficients versus L/B; and (f) critical peak pressure coefficients versus L/B.

remarkable tendency with H/B, compared with that for open terrain, possibly due to the flow field uncertainty for suburban exposure.

Leeward Walls

Fig. 21 depicts the mean and peak leeward wall pressure coefficients for the critical base shear, as a function of H/L, H/B, and L/B. Low-rise buildings are, by definition, shorter than the least horizontal dimension. Leeward walls illustrate the least complete collapse with a single parameter. Chapter 28 with fixed values envelops the load coefficients for many of the buildings, while Chapter 27 is conservative for all buildings, but not economic and accurate because L/B is not the most effective normalization. Examining the figures, either H/B or H/L may be most effective. As mentioned earlier, the leeward wall is less critical for the setting of the base shear coefficient than the windward wall. Given that the leeward pressure for low-rise buildings depends primarily on the roof pressures following reattachment, a constant value may be most appropriate for low-rise buildings, noting that, for the limiting case of $H/L \sim 1$, increased values may be expected because the pressure has not had sufficient distance to recover following reattachment (Akon and Kopp 2016). For this reason, H/L may be the most appropriate nondimensional geometric parameter to capture the leeward pressure coefficients.

Base Shear

Fig. 22 depicts the base shear coefficients relative to H/L, H/B, and L/B. The complexity arises because the windward and leeward walls depend, at least to some extent, on different parameters. Fig. 14 indicates the windward wall is more closely related to the base shear, which makes the peak loads better fit for H/B. Whereas, for the mean values, either H/B or H/L yields a similar

Downloaded from ascelibrary.org by University of Western Ontario on 09/05/22. Copyright ASCE. For personal use only; all rights reserved.

Downloaded from ascelibrary.org by University of Western Ontario on 09/05/22. Copyright ASCE. For personal use only; all rights reserved.

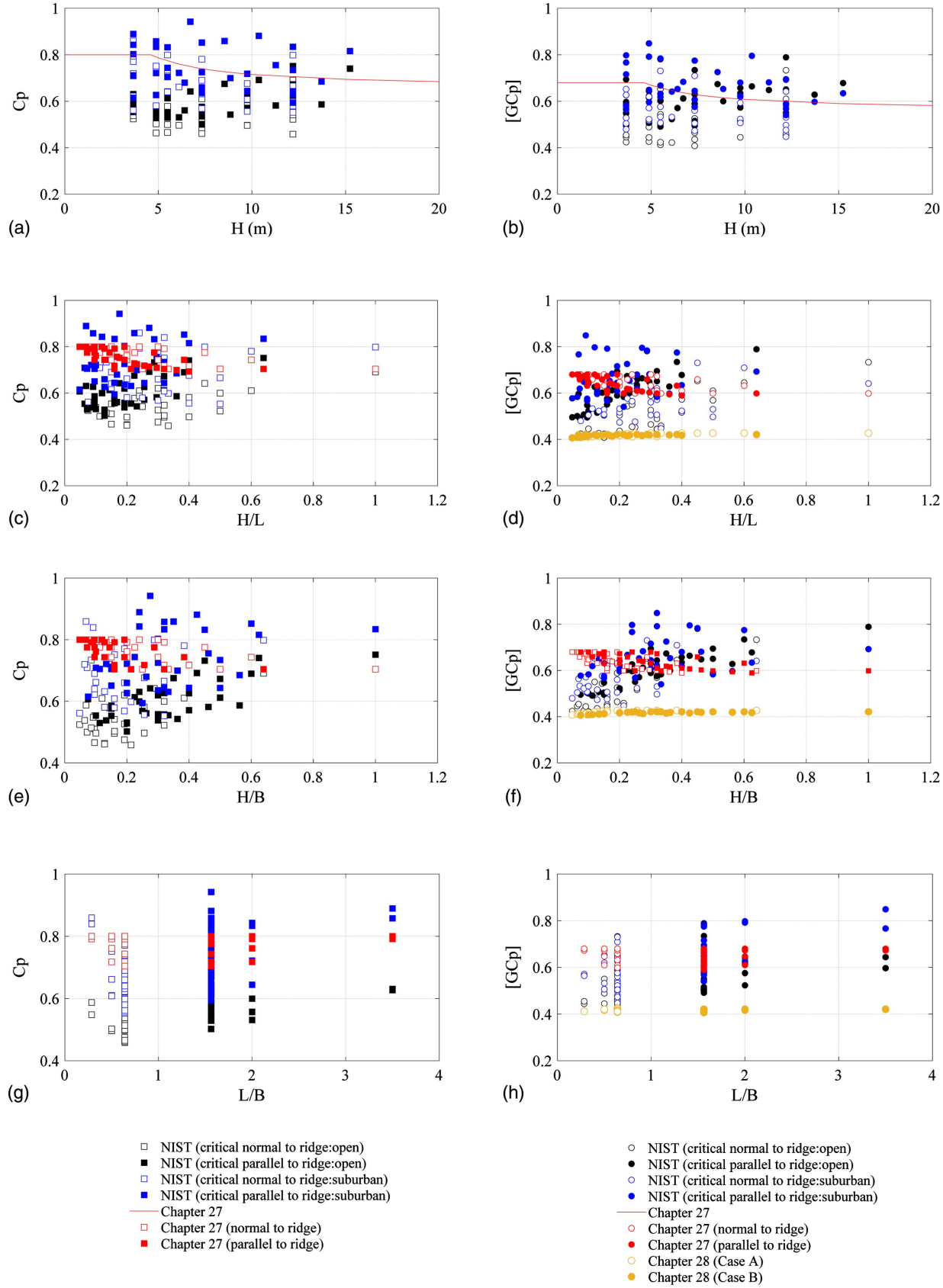

Fig. 20. Critical mean and peak windward wall pressure coefficients: (a) critical mean pressure coefficients versus roof height, H; (b) critical peak pressure coefficients versus roof height, H; (c) critical mean pressure coefficients versus H/L; (d) critical peak pressure coefficients versus H/L; (e) critical mean pressure coefficients versus H/B; (f) critical peak pressure coefficients versus H/B; (g) critical mean pressure coefficients versus L/B; and (h) critical peak pressure coefficients versus L/B.

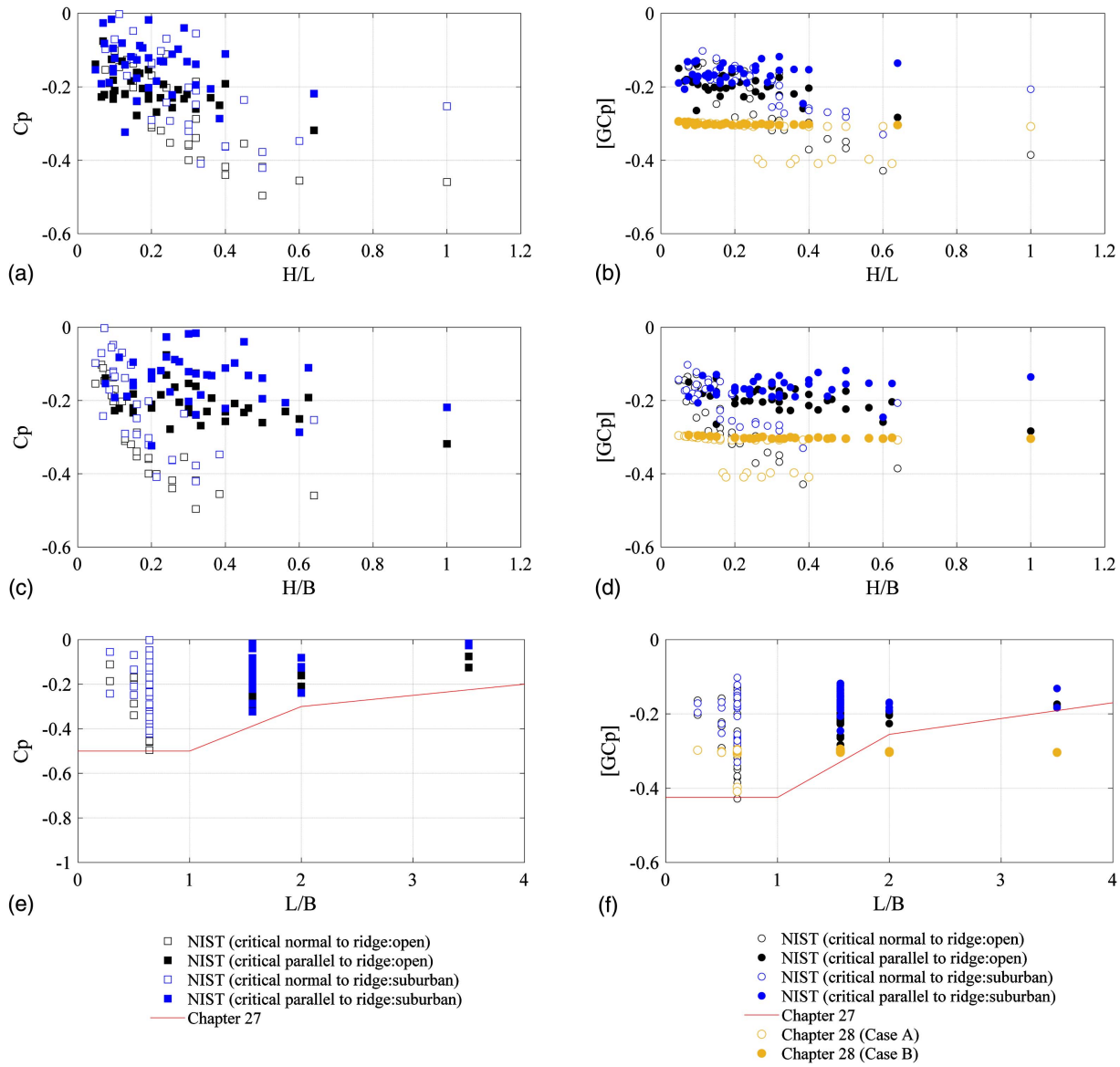

Fig. 21. Mean and peak leeward wall pressure coefficients for the critical base shears versus H/L, H/B, and L/B: (a) critical mean pressure coefficients versus H/L; (b) critical peak pressure coefficients versus H/L; (c) critical mean pressure coefficients versus H/B; (d) critical peak pressure coefficients versus H/B; (e) critical mean pressure coefficients versus L/B; and (f) critical peak pressure coefficients versus L/B.

collapse. The peak base shear exhibits a more distinct tendency with H/B than that for the mean values, indicating distinct trends in the gust-effect factor, which will be examined in a future study.

Conclusions

An examination and validation of the wind load provisions for Chapters 27 and 28 of ASCE 7-16 were conducted by comparing these with the NIST aerodynamic database for low-rise buildings. The mean and peak overall structural load coefficients and area-averaged wall pressure coefficients were analyzed and compared with the code provisions. The key geometric parameters controlling the aerodynamic loads were investigated. The results indicate that ASCE 7-16 cannot conservatively or accurately evaluate the actual wind loads on low-rise buildings for certain building configurations. The main findings are summarized below:

- The provisions of Chapter 27 capture the trend of uplift on roofs as a function roof height, regardless of the roof pitch, and conservatively provide the mean and peak pressure coefficients for the overall roof. The uplift coefficients for open country, with reasonable accuracy, represent those for suburban terrain.
- Base shears obtained from Chapter 27 cannot capture the tendencies of the wind tunnel data for a range of building geometries, although the chapter does conservatively (safely) provide the peak values.
- The provisions of Chapter 27 do not accurately and conservatively assess the peak windward wall pressure coefficients due to inaccuracies in both the mean windward wall pressure coefficients and the gust-effect factor. The wind tunnel results indicate that peak windward wall pressure coefficients tend to be controlled by the wall aspect ratio, H/B, especially for open country.
- The use of the geometric parameter, L/B, in Chapter 27 is not appropriate for determining the leeward wall pressure coefficients on low-rise buildings. Rather, the ratio, H/L, is more appropriate.
- Side wall pressure coefficients vary in a similar way as the uplift, such that the use of the Chapter 27 uplift coefficients would be acceptable as a model for the side wall coefficients.

Downloaded from ascelibrary.org by University of Western Ontario on 09/05/22. Copyright ASCE. For personal use only; all rights reserved.

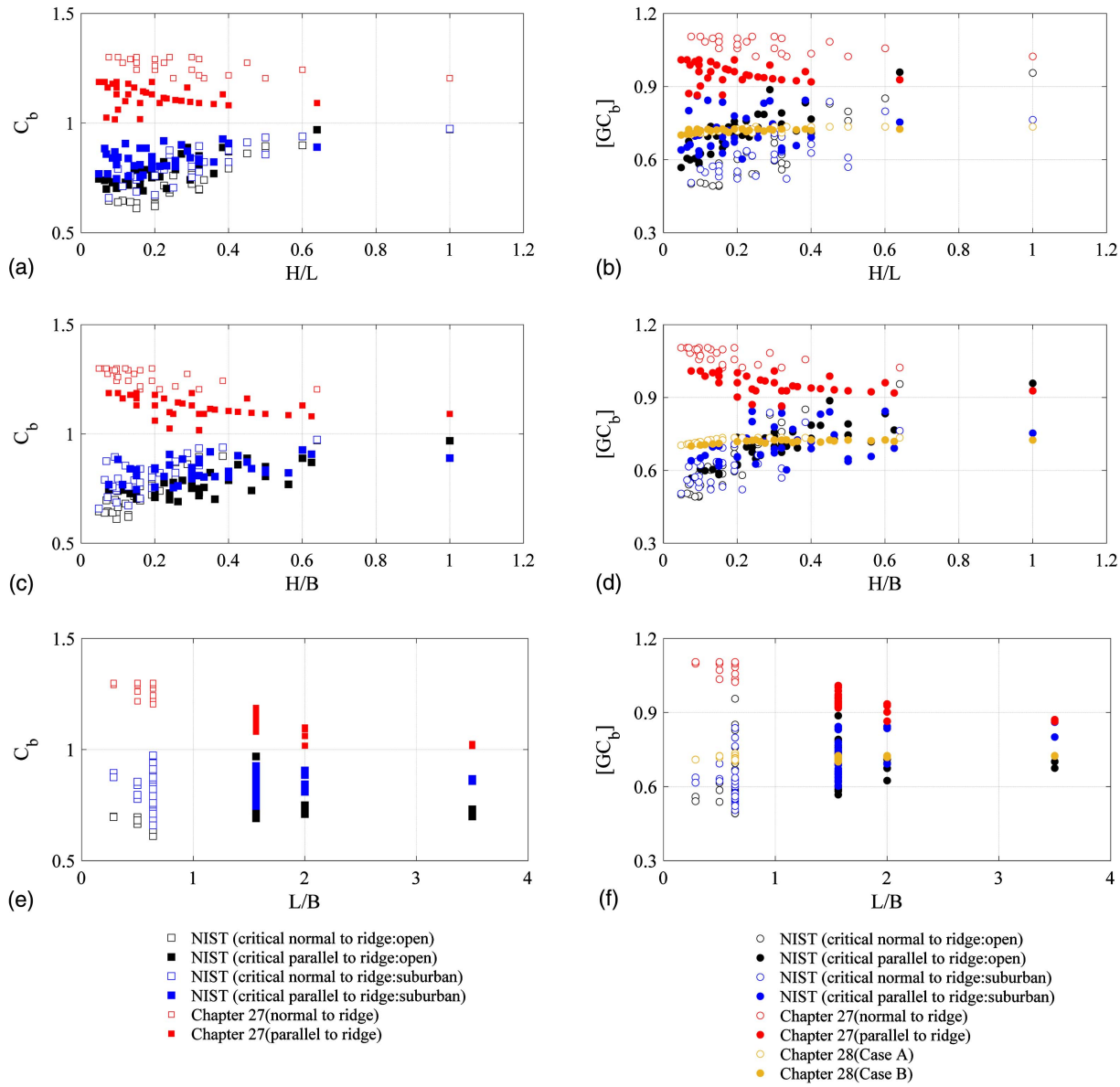

Fig. 22. Critical mean and peak base shears versus H/L, H/B, and L/B: (a) critical mean pressure coefficients versus H/L; (b) critical peak pressure coefficients versus H/L; (c) critical mean pressure coefficients versus H/B; (d) critical peak pressure coefficients versus H/B; (e) critical mean pressure coefficients versus L/B; and (f) critical peak pressure coefficients versus L/B.

- The provisions of Chapter 28 do not capture the tendencies of wind load on building configurations, with the (mostly) fixed load coefficients. As indicated above, the measured data indicate that the roof, side wall, and leeward wall load coefficients depend primarily on H/L, while the windward wall depends primarily on H/B.
- Because Chapter 28 was developed using data from relatively lower low-rise buildings, it does not conservatively envelop the load coefficients on buildings with $H/L > \sim 0.5$. In addition, Chapter 28 significantly underestimates the windward wall pressures for almost all buildings.

Data Availability Statement

Some or all data, models, or code that support the findings of this study are available from the corresponding author upon reasonable request.

Acknowledgments

The authors gratefully acknowledge the partial financial support of the Natural Sciences and Engineering Research Council (NSERC) of Canada through the Discovery Grants program. The authors are grateful to an advisory group made up of members of the ASCE 7-22 Wind Loads Sub-Committee, chaired by Don Scott. GAK gratefully acknowledges the support of ImpactWX and the University of Western Ontario.

References

Akins, R. E., J. A. Peterka, and J. E. Cermak. 1977. "Mean force and moment coefficients for buildings in turbulent boundary layers." *J. Wind Eng. Ind. Aerodyn.* 2 (3): 195–209. https://doi.org/10.1016/0167-6105(77)90022-8.

Akon, A. F., and G. A. Kopp. 2016. "Mean pressure distributions and reattachment lengths for roof-separation bubbles on low-rise buildings."

Downloaded from ascelibrary.org by University of Western Ontario on 09/05/22. Copyright ASCE. For personal use only; all rights reserved.

J. Wind Eng. Ind. Aerodyn. 155 (Aug): 115–125. https://doi.org/10.1016/j.jweia.2016.05.008.

ASCE. 1995. *Minimum design loads for buildings and other structures*. ASCE 7-95. Reston, VA: ASCE.

ASCE. 2002. *Minimum design loads for buildings and other structures*. ASCE 7-02. Reston, VA: ASCE.

ASCE. 2016. *Minimum design loads for buildings and other structures.* ASCE 7-16. Reston, VA: ASCE.

Chiu, G. L., and D. C. Perry. 1997. "Low-rise building wind load provisions: Where are we and where do we need to go?" *Eng. J.* 34 (4): 135–151.

Davenport, A. G., D. Surry, and T. Stathopoulos. 1977. *Wind loads on low-rise buildings: Final report of phases I and II, parts 1 and 2*. BLWT Rep. No. SS8-1977. London, ON, Canada: Univ. of Western Ontario.

Diaz, Q. 2006. "Uncertainty analysis of surface pressure measurements on low-rise buildings." Master's thesis, Dept. of Civil and Environmental Engineering, Univ. of Western Ontario.

ESDU (Engineering Sciences Data Unit). 1982. *Strong winds in the atmospheric boundary layer. Part 1: Mean-hourly wind speeds*. Engineering Sciences Data Unit Item No. 82026. London: ESDU.

ESDU (Engineering Sciences Data Unit). 1983. *Strong winds in the atmospheric boundary layer. Part 2: Discrete gust speeds*. Engineering Sciences Data Unit Item No. 83045. London: ESDU.

Gavanski, E., and Y. Uematsu. 2014. "Local wind pressures acting on walls of low-rise buildings and comparisons to the Japanese and US wind loading provisions." *J. Wind Eng. Ind. Aerodyn.* 132 (Sep): 77–91. https://doi.org/10.1016/j.jweia.2014.06.020.

Ho, T. C. E., D. Surry, D. Morrish, and G. A. Kopp. 2005. "The UWO contribution to the NIST aerodynamic database for wind loads on low buildings. Part 1: Archiving format and basic aerodynamic data." *J. Wind Eng. Ind. Aerodyn.* 93 (1): 1–30. https://doi.org/10.1016/j.jweia.2004.07.006.

Holmes, J., Y. Tamura, and P. Krishna. 2009. "Comparison of wind loads calculated by fifteen different codes and standards, for low, medium and high-rise buildings." In *Proc., 11th Americas Conf. on Wind Engineering*. Ft. Collins, CO: American Association of Wind Engineering.

Holmes, J. D. 2014. "Along- and cross-wind response of a generic tall building: Comparison of wind-tunnel data with codes and standards." *J. Wind Eng. Ind. Aerodyn.* 132 (Sep): 136–141. https://doi.org/10.1016/j.jweia.2014.06.022.

Holmes, J. D., C. J. Baker, E. C. English, and E. C. C. Choi. 2005a. "Wind structure and codification." *Wind Struct.* 8 (4): 235–250. https://doi.org/10.12989/was.2005.8.4.235.

Holmes, J. D., M. Kasperski, C. A. Miller, J. A. Zuranski, and E. C. C. Choi. 2005b. "Extreme wind prediction and zoning." *Wind Struct.* 8 (4): 269–281. https://doi.org/10.12989/was.2005.8.4.269.

Hong, E. S. 2017. "Wall pressure coefficients for low- to high-rise buildings." Master dissertation, Faculty of Graduate Studies, Univ. of Western Ontario.

Kasperski, M. 1996. "Design wind loads for low-rise buildings: A critical review of wind load specifications for industrial buildings." *J. Wind Eng. Ind. Aerodyn.* 61 (2–3): 169–179. https://doi.org/10.1016/0167-6105(96)00051-7.

Kasperski, M., and C. Geurts. 2005. "Reliability and code level." *Wind Struct.* 8 (4): 295–307. https://doi.org/10.12989/was.2005.8.4.295.

Kopp, G. A., and M. J. Morrison. 2018. "Component and cladding wind loads for low-slope roofs on low-rise buildings." *J. Struct. Eng.* 144 (4): 04018019. https://doi.org/10.1061/(ASCE)ST.1943-541X.0001989.

Letchford, C., J. D. Holmes, R. Hoxey, and A. Robertson. 2005. "Wind pressure coefficients on low-rise structures and codification." *Wind Struct.* 8 (4): 283–294. https://doi.org/10.12989/was.2005.8.4.283.

Levitan, M. L., and K. C. Mehta. 1992. "Texas Tech field experiments for wind loads. Part 1: Building and pressure measuring system." *J. Wind Eng. Ind. Aerodyn.* 43 (1–3): 1565–1576. https://doi.org/10.1016/0167-6105(92)90372-H.

Lieblein, J. 1976. *Efficient methods of extreme-value methodology.* Rep. No. NEA-CSNI-R–1976-10. Washington, DC: National Bureau of Standards.

Liu, Y., G. A. Kopp, and S. F. Chen. 2019. "Effects of plan dimensions on gust wind loads for high-rise buildings." *J. Wind Eng. Ind. Aerodyn.* 194 (Nov): 103980. https://doi.org/10.1016/j.jweia.2019.103980.

Lopez, C., and F. Masters. 2010. "Flow measurement, analysis and simulation of wind-driven rain for engineering applications." In *Proc., 2nd Workshop of the American Association for Wind Engineering (AAWE)*. Ft. Collins, CO: American Association of Wind Engineering.

Oh, J. H., G. A. Kopp, and D. R. Inculet. 2007. "The UWO contribution to the NIST aerodynamic database for wind loads on low buildings. Part 3: Internal pressures." *J. Wind Eng. Ind. Aerodyn.* 95 (8): 755–779. https://doi.org/10.1016/j.jweia.2007.01.007.

Simiu, E., C. Letchford, N. Isyumov, A. G. Chowdhury, and D. Yeo. 2012. "Assessment of ASCE 7-10 standard methods for determining wind loads." *J. Struct. Eng.* 139 (11): 2044–2047. https://doi.org/10.1061/(ASCE)ST.1943-541X.0000771.

Solari, G. 1993a. "Gust buffeting. I: Peak wind velocity and equivalent pressure." *J. Struct. Eng.* 119 (2): 365–382. https://doi.org/10.1061/(ASCE)0733-9445(1993)119:2(365).

Solari, G. 1993b. "Gust buffeting. II: Dynamic alongwind response." *J. Struct. Eng.* 119 (2): 383–398. https://doi.org/10.1061/(ASCE)0733-9445(1993)119:2(383).

Solari, G., and A. Kareem. 1998. "On the formulation of ASCE 7-95 gust-effect factor." *J. Wind Eng. Ind. Aerodyn.* 77 (Sep): 673–684. https://doi.org/10.1016/S0167-6105(98)00182-2.

Stathopoulos, T. 1979. "Turbulent wind action on low-rise buildings." Ph.D. thesis, Dept. of Civil and Environmental Engineering, Univ. of Western Ontario.

Stathopoulos, T. 2003. "Wind loads on low buildings: In the wake of Alan Davenport's contributions." *J. Wind Eng. Ind. Aerodyn.* 91 (12–15): 1565–1585. https://doi.org/10.1016/j.jweia.2003.09.019.

St. Pierre, L. M., G. A. Kopp, D. Surry, and T. C. E. Ho. 2005. "The UWO contribution to the NIST aerodynamic database for wind loads on low buildings. 2: Comparison of data with wind load provisions." *J. Wind. Eng. Ind. Aerodyn.* 93 (1): 31–59. https://doi.org/10.1016/j.jweia.2004.07.007.

Tamura, Y., A. Kareem, G. Solari, K. Kwok, J. D. Holmes, and W. H. Melbourne. 2005. "Aspects of the dynamic wind-induced response of structures and codification." *Wind Struct.* 8 (4): 251–268. https://doi.org/10.12989/was.2005.8.4.251.

Tieleman, H. W. 2003. "Wind tunnel simulation of wind loading on low-rise structures: A review." *J. Wind Eng. Ind. Aerodyn.* 91 (12–15): 1627–1649. https://doi.org/10.1016/j.jweia.2003.09.021.

Wu, C. H., and G. A. Kopp. 2018. "A quasi-steady model to account for the effects of upstream turbulence characteristics on pressure fluctuations on a low-rise building." *J. Wind Eng. Ind. Aerodyn.* 179 (Aug): 338–357. https://doi.org/10.1016/j.jweia.2018.06.014.

Downloaded from ascelibrary.org by University of Western Ontario on 09/05/22. Copyright ASCE. For personal use only; all rights reserved.